5. Electron Transfer and Solvation Dynamics at the NH_3/Cu(111) Interface

This chapter presents the electron transfer and solvation dynamics of the NH_3/Cu(111) system. It is shown that the underlying fundamental processes of charge injection, trapping and back relaxation are in principle analogous to the dynamics at ice-metal interfaces. However, distinct differences are found, which are characteristic for the new solvent. In the case of amorphous ammonia (cf. section 5.1), for example, the electron transfer is considerably slowed down compared with amorphous ice, so that investigation of the excess electron's dynamics up to 300 ps is enabled. As water, also ammonia exhibits a structural transition to the crystalline phase as introduced in 2.4.1. The crystallization, which is observed at 100 K by TD spectroscopy (cf. 3.3.2), is accompanied by significant changes in the electron transfer and solvation dynamics. (cf. section 5.2) Pump-probe experiments up to minute timescales are possible, revealing that the occurrence of an ultralong-living trapped electron state is not an ice-specific feature, but of a more general character.

5.1 Ultrafast Electron Dynamics in Amorphous Ammonia Adlayers

As introduced in section 3.3.2, amorphous ammonia adlayers are deposited at a sample temperature of 30 K. The following paragraph shows that the fundamental steps of charge injection, solvation, and back transfer are comparable to the amorphous ice-metal interfaces discussed in chapter 4. However, the electron dynamics are considerably slowed down and exhibit a pronounced coverage dependence resulting from the surface-bound character of the excess electrons (cf. 5.1.2). Paragraph 5.1.3 shows that – in contrast to the ice-metal systems – the electron transfer dynamics depend significantly on temperature. This finding in combination with the coverage dependence of electron tunneling enables tuning of the coupling degree of the ammoniated electrons to the Cu(111) substrate.

5.1.1 Formation Dynamics of Solvated Electrons

Fig. 5.01 presents the time- (bottom axes) and energy-resolved (vertical axis) 2PPE results of an 8.5 ML thick amorphous NH_3 film on the Cu(111) surface in false color representation (intensity scale in the right panel). As in the case of D_2O, two features are observed: (i) A

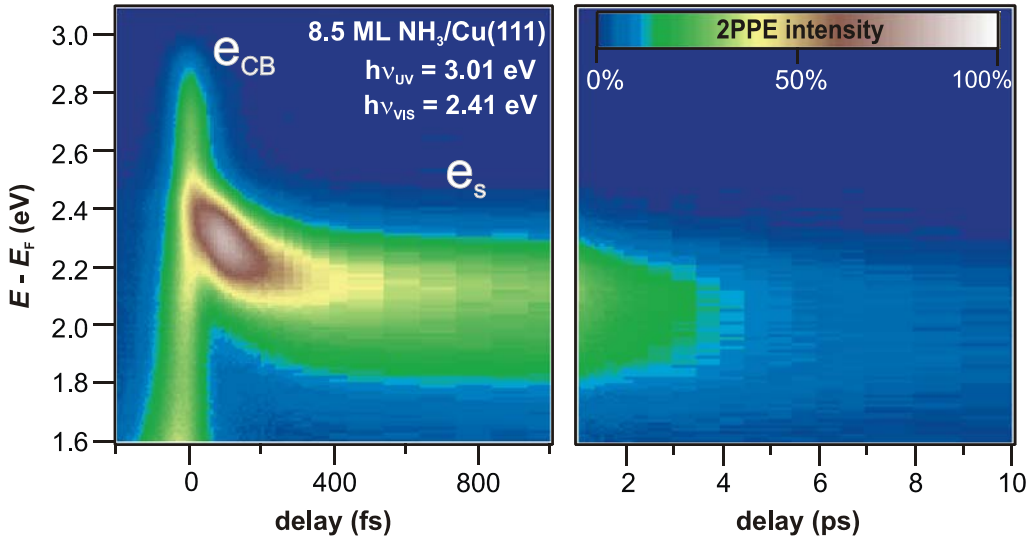

Fig. 5.01: *Time-Resolved 2PPE Data of 8.5 ML Amorphous NH_3/Cu(111).* 2PPE intensity in false color representation as a function of intermediate state energy and pump-probe time delay. In accordance with the ice-metal interfaces, the spectra exhibit a short-lived continuum, e_{CB}, attributed to the ammonia conduction band and a peak e_S, shifting to lower energies with increasing time delay, which is associated with solvated electrons in the NH_3 adlayer.

broad, short-lived continuum and (ii) a peak that exhibits a finite lifetime and shifts down to lower energies with increasing time delay. Note, that this feature is excited by $h\nu_{UV}$ = 3.01 eV, probed by VIS photons, and exhibits an intermediate state energy of 2.4 eV. However, as apparent from Fig. 5.01 at negative delays, the state is *not* excited by $h\nu_{VIS}$ = 2.41 eV. In accordance with the electron dynamics at ice-metal interfaces it is concluded, that the electrons are excited via the energetically higher lying conduction band of the NH_3 adlayer, e_{CB}, i.e. requiring photon energies > 2.4 eV. Subsequently, the electron is localized by the solvent molecules leading to the spectral feature e_S of the solvated electrons.[95] However, the data exhibit also strong differences compared with ice-metal interfaces. As apparent by the femtosecond dynamics in the left panel of Fig. 5.01, the peak shift slows down significantly after 300 fs. In addition, the back transfer of the solvated electron population back to the metal substrate occurs much slower than for amorphous D_2O/Cu(111), so that the electron can even be monitored on picosecond timescales (right panel). A quantitative analysis of the energetic shift of the peak maximum is given in Fig. 5.02, the electron transfer dynamics are discussed later, on the basis of Fig. 5.03.

The position of the peak maximum of the solvated electron distribution was determined manually as for the ice-metal interfaces (cf. 4.1.1). As apparent by the inset of Fig. 5.02a, the maximum of e_S lies at to $E - E_F$ = 2.38(2) eV right after photoexcitation at t = 0 fs. A linear fit to the data shows that the maximum of e_S shifts initially with a rate of Σ_S^I = -0.80(5) eV/ps down to lower energies. As the e_S population *increases* during the first few hundred fs as

[95] Dispersion measurements discussed in appendix A show the localized character of e_S.

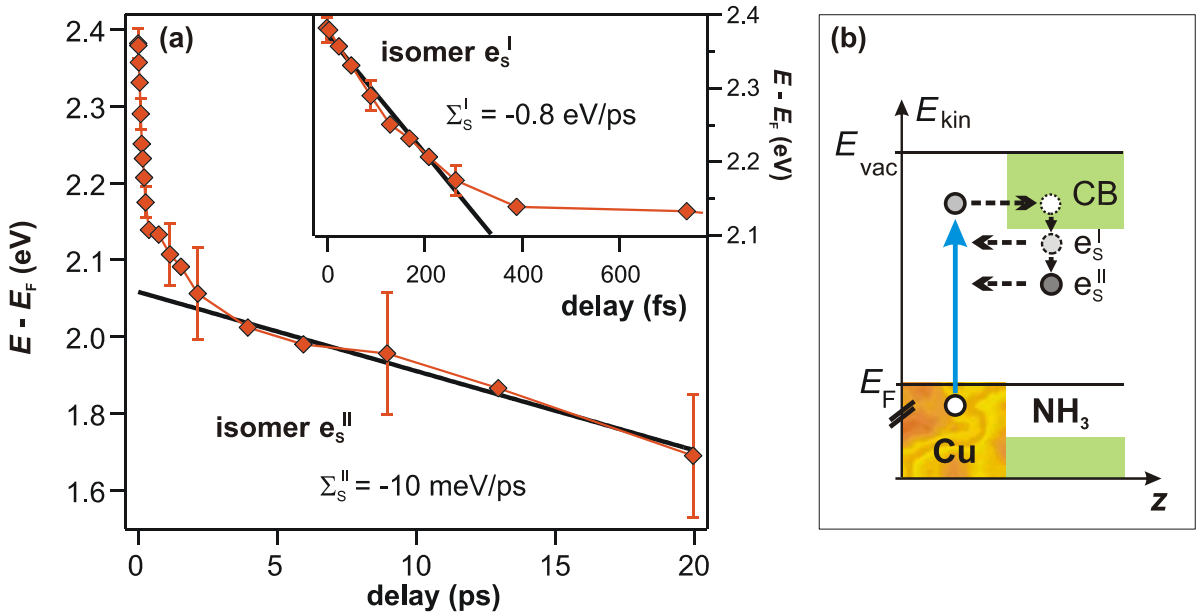

Fig. 5.02: *Shift of Peak Maximum of 8.5 ML Amorphous NH_3/Cu(111).* a) The peak maximum of e_S (markers) shifts at early delays (<300 fs, inset) 100 times faster to lower energies than in the late time regime (t > 3 ps) as apparent by the linear fits (solid lines). b) Electron solvation in NH_3 adlayers via two isomers. See text for details.

apparent from Fig. 5.01, the main contribution to the peak shift is due to the energetic stabilization of the solvated electrons. However, an additional, *apparent* peak shift due to energy-dependent transfer times as in the case of amorphous ice-metal interfaces might also influence the peak shift. Though, after $t \approx 300$ fs, the shift slows significantly down. For pump-probe delays > 3 ps the peak shift is with Σ_S^{II} = -10(1) meV/ps almost 100 times slower than in the early time regime. Apparently, the electron solvation occurs via two different states, which exhibit stabilization dynamics on femto- and on picosecond timescales, respectively. Fig. 5.02b illustrates a possible scenario for electron solvation in amorphous NH_3 adlayers on Cu(111). After injection to the NH_3 conduction band, the electrons localize in isomer e_S^I, which exhibits a peak shift on femtosecond timescales. After 300 fs, a transition to the second isomer e_S^{II} occurs, which is accompanied by a considerable slowing down of the peak shift.[96] Before turning to an interpretation of this scenario, the population dynamics of the solvated electrons in NH_3/Cu(111) are discussed in the following.

Fig. 5.03a presents the population transient of the solvated electrons.[97] The population decay for late delays (>3 ps) is very well fitted by a single exponential decay (blue line) with the time constant of 6.2 ps. At earlier delays (inset) a more sophisticated analysis is required. A two-level system consisting of the CB and *one* solvated electron state e_S as introduced in 4.2.1 is

[96] In agreement with literature, where different solvated electron states are termed isomers (e.g. for surface- and bulk-bound electrons in gas phase clusters [Ver05a]), e_S^I and e_S^{II} are also referred to as isomers, although the number of molecules contributing to the solvation shell is not known.

[97] The transient is achieved by integrating the 2PPE intensity of the dataset in Fig. 5.01 over the energy window of $E - E_F$ = 1.4 eV to 2.7 eV.

depicted in Fig. 5.03b. Assuming the excitation probabilities 1-p and p, a decay rate Γ_{eS}, and the localization probability Γ_{loc}, the population of e_S should follow the rate equation[98]

$$\frac{\partial n_{eS}}{\partial t} = -\Gamma_{eS} \cdot n_{eS} + \Gamma_{loc} \cdot n_{CB} \qquad \text{with} \qquad \frac{\partial n_{CB}}{\partial t} = -\Gamma_{loc} \cdot n_{CB} \tag{5.1}$$

with the solution

$$n_{eS}(t) = \frac{p\Gamma_{eS} - \Gamma_{loc}}{\Gamma_{eS} - \Gamma_{loc}} \cdot \exp[-\Gamma_{eS} \cdot t] + \frac{(1-p)\Gamma_{loc}}{\Gamma_{eS} - \Gamma_{loc}} \cdot \exp[-\Gamma_{loc} \cdot t]. \tag{5.2}$$

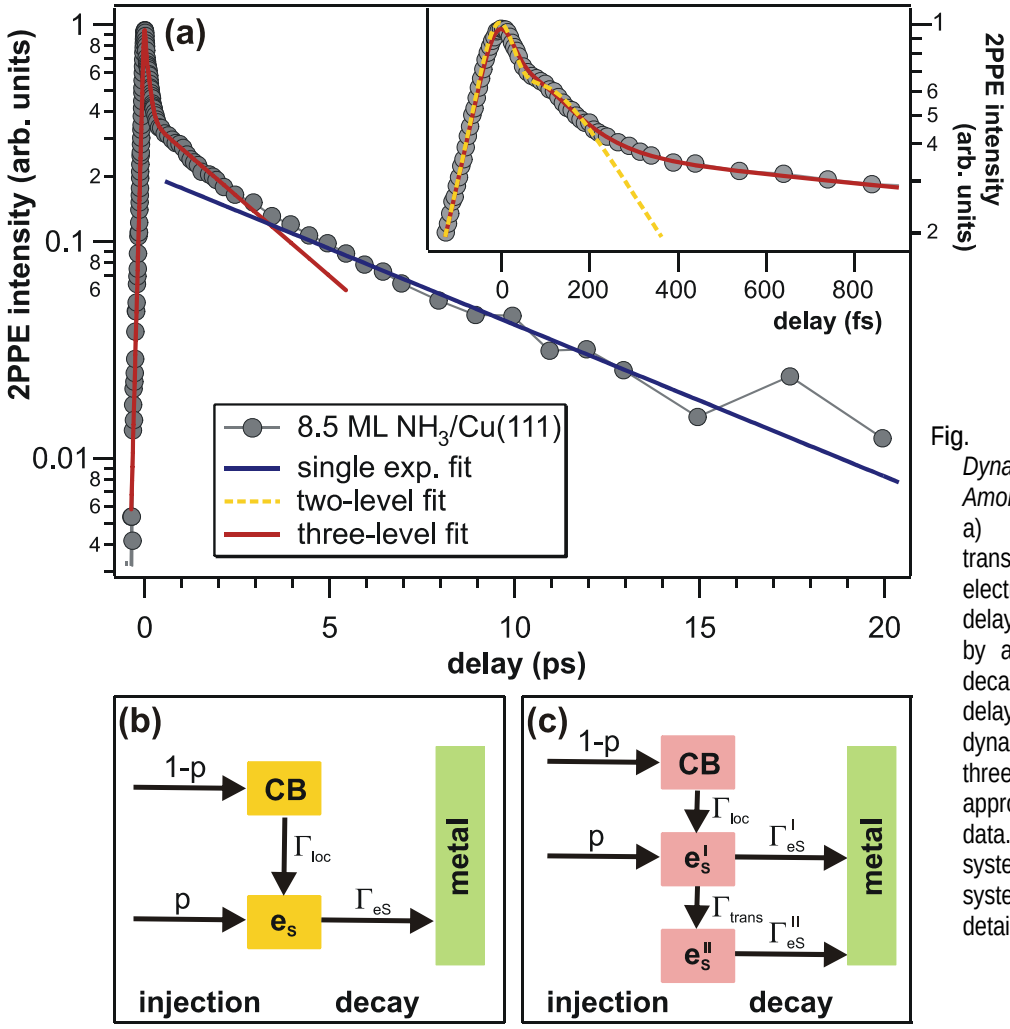

Fig. 5.03: *Population Dynamics of 8.5 ML Amorphous NH_3/Cu(111).* a) The population transient of the solvated electron state is at late delays reproduced well by a single exponential decay (blue line). At early delays (inset) population dynamics of a two- and a three-level rate equation approach are fitted to the data. b) Two-level system. c) Three-level system. See text for details.

[98] The applicability of rate equations – instead of optical Bloch Equations – to the population dynamics of solvated electrons has been shown in 3.4.2.

The dotted orange curve (least square fit, inset of Fig. 5.03a) results, when including an exponential decrease to negative delays to account for the hot electrons and convolving the resulting function with the laser pulses envelope. As apparent from the figure, the above description indeed can describe the delayed rise of the e_S population at 150 fs, but not the deceleration of population decay after 300 fs. Therefore, a three-level system is developed, taking into account the CB and *two* isomers of solvated electrons, one representing the fast dynamics for t < 300 fs, e_S^I, and the other describing the slow dynamics for larger delays (> 300 fs). As depicted in Fig. 5.03c excitation probabilities 1-p and p, decay rates Γ_{eS}^{I} and Γ_{eS}^{II}, the localization probability Γ_{loc}, and a transition probability from e_S^I to e_S^{II}, Γ_{trans}, are implemented leading to the rate equations

$$\frac{\partial n_{CB}}{\partial t} = -\Gamma_{loc} \cdot n_{CB} \quad \text{with} \quad n_{CB}(0) = 1 - p \tag{5.3a}$$

$$\frac{\partial n_{eS}^{I}}{\partial t} = -\left(\Gamma_{eS}^{I} + \Gamma_{trans}\right) \cdot n_{eS}^{I} + \Gamma_{loc} \cdot n_{CB} \quad \text{with} \quad n_{eS}^{1}(0) = p \tag{5.3b}$$

$$\frac{\partial n_{eS}^{II}}{\partial t} = -\Gamma_{eS}^{II} \cdot n_{eS}^{II} + \Gamma_{trans} \cdot n_{eS}^{I} \quad \text{with} \quad n_{eS}^{II}(0) = 0 \tag{5.3c}$$

with the solutions

$$n_{CB}(t) = (1 - p) \cdot \exp\left[-\Gamma_{loc} \cdot t\right] \tag{5.4a}$$

$$n_{eS}^{I}(t) = \underbrace{\frac{p\left(\Gamma_{eS}^{I} + \Gamma_{trans}\right) - \Gamma_{loc}}{\Gamma_{eS}^{I} + \Gamma_{trans} - \Gamma_{loc}}}_{A} \cdot \exp\left[-\left(\Gamma_{eS}^{I} + \Gamma_{trans}\right) \cdot t\right] + \underbrace{\frac{(1-p)\Gamma_{loc}}{\Gamma_{eS}^{I} + \Gamma_{trans} - \Gamma_{loc}}}_{B} \cdot \exp\left[-\Gamma_{loc} \cdot t\right] \tag{5.4b}$$

$$n_{eS}^{II}(t) = \frac{\Gamma_{trans}}{\Gamma_{eS}^{II} - \left(\Gamma_{eS}^{I} + \Gamma_{trans}\right)} \cdot A \cdot \left\{e^{-\left(\Gamma_{eS}^{I} + \Gamma_{trans}\right)t} - e^{-\Gamma_{eS}^{II} \cdot t}\right\} + \frac{\Gamma_{trans}}{\Gamma_{eS}^{II} - \Gamma_{loc}} \cdot B \cdot \left\{e^{-\Gamma_{loc} \cdot t} - e^{-\Gamma_{eS}^{II} \cdot t}\right\}. \tag{5.4c}$$

The resulting least square fit (including the hot electron background) is given by the red curve in Fig. 5.03a. It perfectly reproduces the delayed intensity rise, the fast, and the slow component of population decay up to 3 ps resulting in the fit parameters given in Tab. 5.01.

direct excitation probability of e_S^I	p	0
CB → e_S^I	$\tau_{loc} = (\Gamma_{loc})^{-1}$	38(5) fs
e_S^I → e_S^{II}	$\tau_{trans} = (\Gamma_{trans})^{-1}$	220(5) fs
e_S^I → metal	$\tau_{eS}^{I} = (\Gamma_{eS}^{I})^{-1}$	130(5) fs
e_S^{II} → metal	$\tau_{eS}^{II} = (\Gamma_{eS}^{II})^{-1}$	2.96(2) ps

Tab. 5.01: *Fit Parameters for the Population Decay of 8.5 ML Amorphous NH_3/Cu(111).*

It is found that the excitation of the solvated electron state occurs to 100 % via the conduction band (p = 0). The excess electrons localize with a time constant of 38 fs and the transition to the second isomer occurs within 220 fs. In parallel with the localization and transition, the solvated electrons decay back to the metal substrate with characteristic times of $(\Gamma_{eS}^{I})^{-1} = \tau_{eS}^{I}$ = 130 fs and $(\Gamma_{eS}^{II})^{-1} = \tau_{eS}^{II}$ = 3 ps for isomer

e_S^I and e_S^{II}, respectively.

The combination of these results with the observation of a two-component peak shift in Fig. 5.02 enables primary interpretation of the time-resolved 2PPE results of the 8.5 ML amorphous NH_3/Cu(111) interface. Apparently, excess electrons solvate in ammonia layers after photoinjection via two different isomers exhibiting dynamics on different timescales: While e_S^I shifts with a rate of 0.8 eV/ps to lower energies and decays with a time constant of 130 fs back to the metal substrate, the second isomer e_S^{II} exhibits ps dynamics both in peak shift and population decay. It is noteworthy that the initial transfer time τ_{eS}^{I} agrees very well with the initial decay time of solvated electrons in amorphous *ice* on the Cu(111) surface τ_1^{Cu} = 140 fs observed in paragraph 4.1.1. Apparently, the degree of screening of the excess electrons is in this regime comparable for ice and ammonia adlayers at these early stages of solvation. However, the transfer dynamics slow significantly down at later delays for the NH_3/Cu(111) system. Such abrupt change cannot be explained by a steady increase of a tunneling barrier as it was the case for D_2O. A reaction of the surrounding NH_3 molecules on the timescale of τ_{trans} has to occur, that leads to (i) a significant deceleration of electron transfer from fs to ps and (ii) to a slowing down of the electron stabilization.

Snyder and Castleman observed by time-resolved, mass-selective spectroscopy on $(NH_3)_{n<40}$ clusters that proton transfer between an excited ammonia molecule (the H-bond donor) and another NH_3 (the H-bond acceptor)

$$(NH_3)^* \rightarrow NH_2^- \bullet H^+(NH_3)_{n-1} \tag{5.5}$$

occurs with a time constant of 135 fs for $n > 11$ at ~249 K. [Sny97] This proton transfer time is in the same order of magnitude as the transition time τ_{trans} = 220 fs observed here at 30 K. Assuming a solvated electron of isomer e_S^I after photoinjection via the CB, localized in the ammonia layer, being subsequently stabilized by a reorientation of the surrounding molecules, might well initiate a proton transfer towards the electron due to its electric field. Such transfer will result in a drop of the electron energy and a smaller net electric field that would have to be screened from the metal substrate; the decay probability would decrease immediately. A transferred proton being the reason for the sudden slowing down of electron dynamics after 300 fs is thus a reasonable scenario. However, proton transfer reactions are known to occur generally faster in water-ice than in ammonia. [99] [Tho81] The question arises, why an $e_S^I \rightarrow e_S^{II}$ transition is not observed for the ice-metal interfaces investigated in this work. A possible explanation could be a larger localization of the excess electrons in NH_3 than in D_2O layers on metal surfaces, which would result in a higher electric field that could drive the proton transfer reaction.

However, it has to be concluded, that the underlying mechanism for the $e_S^I \rightarrow e_S^{II}$ transition remains undetermined. As the two isomers are not observed for the ice-metal interfaces, it either is an NH_3 specific feature or the fast decay of solvated electrons in amorphous ice prohibits its occurrence. Another possible candidate, besides the proton transfer

[99] Studies were performed on crystalline ammonia and water ice.

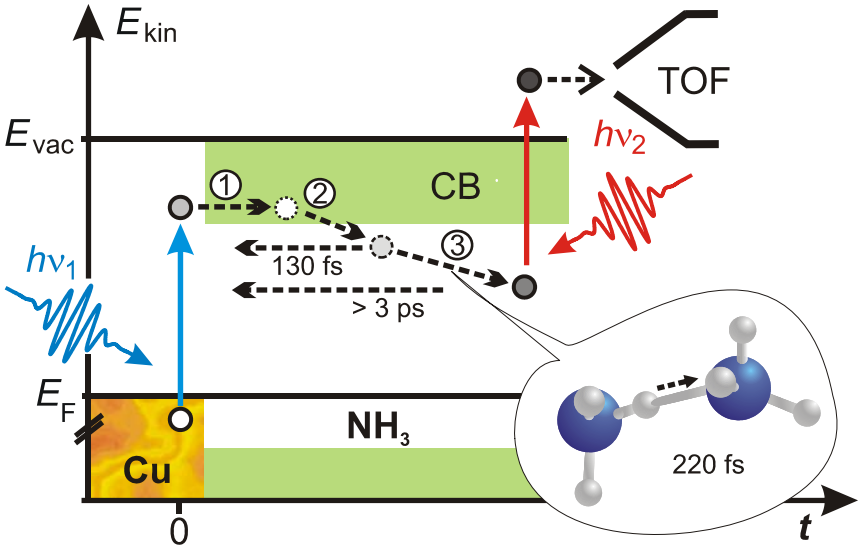

Fig. 5.04: *Fundamental Steps of Electron Solvation in Amorphous NH_3/Cu(111).* Metal electrons are excited and transferred to the NH_3 CB (1). They localize below the bottom of the band (2) and presumably a solvent rearrangement (for example proton transfer) leads to a significant decelaration of electron dynamics (3).

reaction, would be the *umbrella mode* of NH_3, which is the tunneling of the nitrogen atom from one side of the hydrogen triangle to the other. It occurs in ammonia clusters with a frequency of 840 cm^{-1} corresponding to a cycle duration of 40 fs. Also the weaker hydrogen-bonding in ammonia compared with water (cf. 2.3.1) yields an explanation for the transition: Possibly, the strong electric field of the excess charge leads to a cleavage of H-bonds. Resulting dangling protons could contribute to the solvation shell.

The course of events sketched in Fig. 5.04 is – based on the above data analysis – proposed for the NH_3/Cu(111) system: Metal electrons are excited by UV pulses and transferred to the ammonia conduction band (1). Their localization at favorable sites in the adlayer occurs within 40 fs (2). Subsequently, their dynamics slow down drastically. The excess electrons are additionally screened by a structural reorientation occurring within 220 fs. Possible candidates are proton tunneling towards the solvation shell or NH_3 reorientation mediated by the umbrella mode (3). Further stabilization and electron decay are accordingly slower and occur on picosecond timescales, as the driving force (the electric field) is lowered.

Having introduced the fundamental steps of charge transfer and solvation in amorphous ammonia layers on the Cu(111) surface, the next paragraph focuses on the dependence of these dynamics on the NH_3 layer thickness. It is shown that the electron decay time at late delays depends exponentially on coverage, suggesting electron solvation at the ammonia-vacuum *interface* and tunneling-mediated HET.

5.1.2 Charge Transfer Mediated by Tunneling

In contrast to amorphous D_2O/Cu(111), where for layer thicknesses above 3 BL no coverage dependence of work function and solvated electron dynamics was observed, the electron dynamics of the NH_3/Cu(111) system indeed exhibit differences. Fig. 5.05a presents the coverage dependence of the work function of NH_3 multilayers on the Cu(111) surface,

adsorbed at 30 K. Adsorption of 2 ML NH_3 reduces Φ from 4.95 eV of bare Cu(111) to 3.51(2) eV. This decrease is – as discussed in 2.4.3 – due to a significant charge transfer from the adsorbate to the substrate and the dipole moment of the NH_3 molecules. However, up to 6 ML the work function decreases further and saturates at 3.31(2) eV. For coverages above 15 ML the work function rises again up to 3.58(2) eV for 26 ML. Conclusions from this coverage dependent behavior have to be treated with caution, however. The initial drop ($\Theta < 6$ ML) is probably due to a net dipole orientation initiated by the adsorption geometry of the ammonia and the charge transfer from nitrogen atoms to the substrate upon binding. For higher coverages (6 ML < Θ < 15 ML) the preferable orientation is lost and the dipole moments are evenly distributed so that Φ does not change with further adsorption. In addition a clustering of the NH_3 molecules as in the case of D_2O/Cu(111) can contribute to the work function increase at the low adsorption temperature of 30 K. The measured work function for Θ < 6 ML would be an averaged value of bare Cu(111) patches and the ammonia cluster-

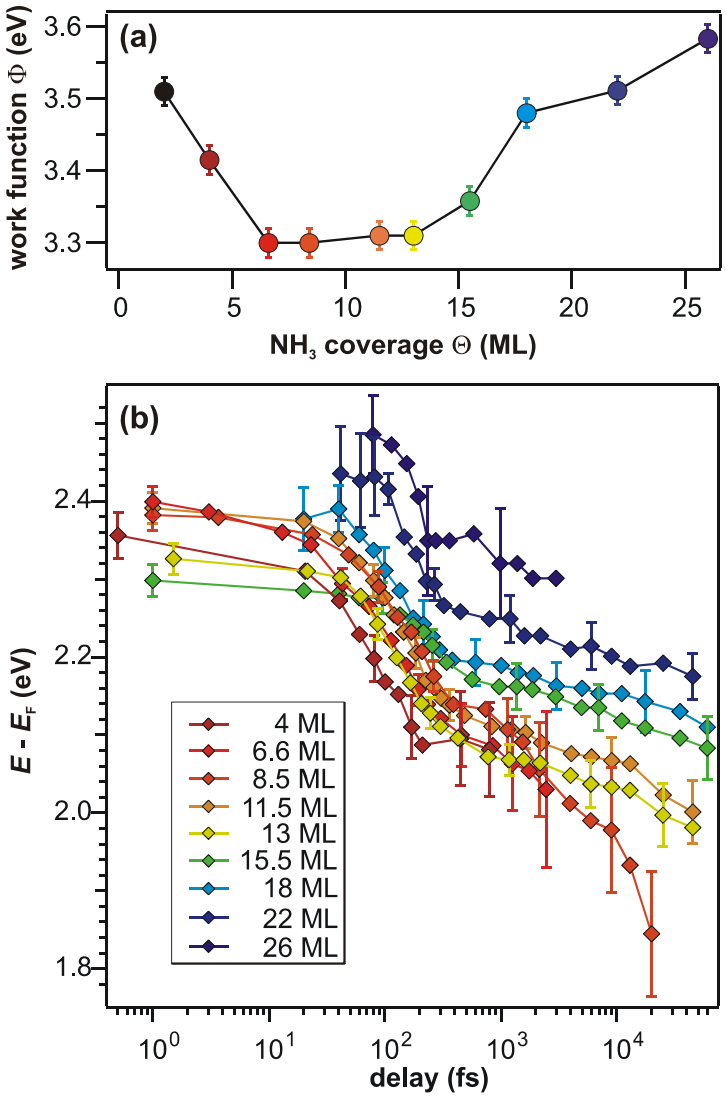

Fig. 5.05: *Coverage Dependence of Work Function and Peak Shift.* a) The work function decreases with rising layer thickness and saturates at 6 ML. For Θ > 15 ML it increases again. b) Peak shift of the solvated electron feature as a function of coverage. Qualitatively, all datasets exhibit the same behavior, characterized by a fast shift for t < 300 fs and a considerably slower stabilization for larger delays. The energetic position of the peak maximum with respect to the Cu(111) Fermi Level increases with rising coverage at all time delays.

covered surface, reaching saturation when the metal surface is completely covered with NH_3. This scenario is supported by the occurrence of the $n = 1$ image potential state of Cu(111) for $\Theta < 6$ ML.[100] The work function rise for even higher coverages ($\Theta > 15$ ML) is however not easily explained. One possible scenario could be an approximation of the sample work function to the ionization energy of bulk ammonia (~10 eV for ammonia clusters [Rei93]).

Besides this work function change also the electron solvation dynamics exhibit a coverage dependence as depicted in Fig. 5.05b. The time-dependent peak shift of the solvated electron distribution is plotted with respect to the Cu(111) Fermi Level for different coverages ranging from 4 (red) to 26 ML (blue).[101] Note the logarithmic time axis, which is used to ensure observation of electron dynamics on all time scales. In all datasets the peak shift is on the order of ~1 eV/ps for $t < 300$ fs and slows significantly down to ~10 meV/ps for larger delays. However, the absolute peak position of e_S with respect to E_F increases with rising coverage at all time delays.[102]

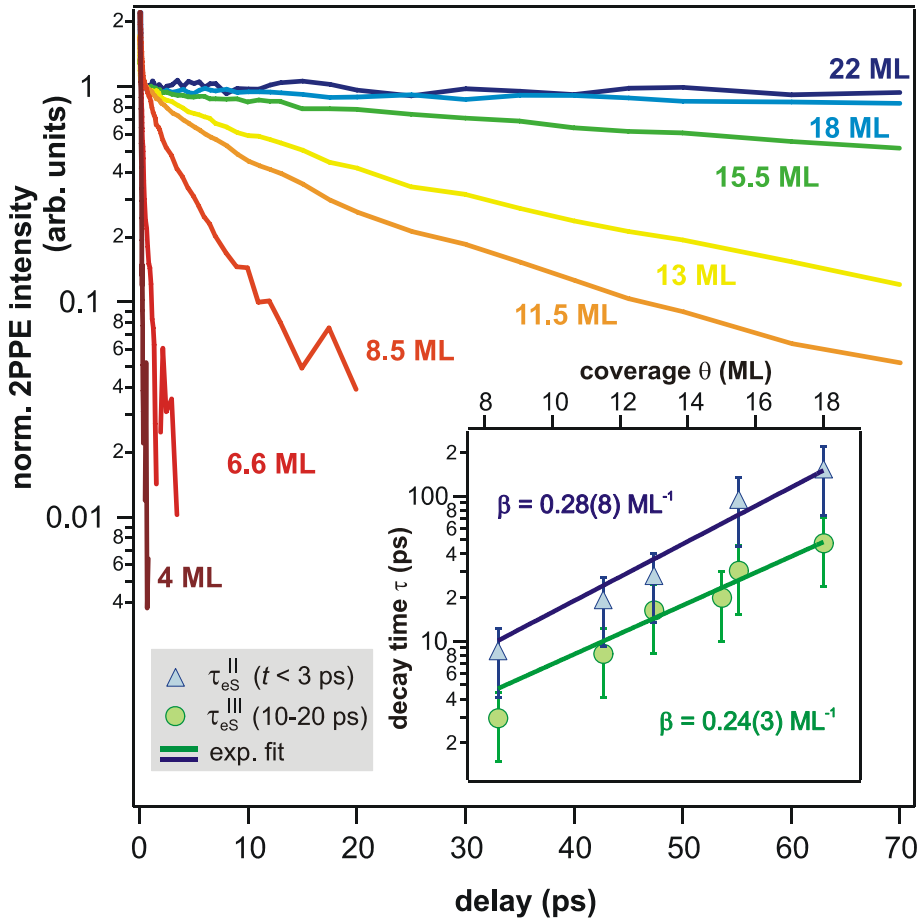

Fig. 5.06: *Coverage Dependence of Population Decay.* The solvated electron population decay in the late time regime slows significantly down with increasing NH_3 coverage and stops for $\Theta >$ 18 ML. Inset: The decay times for delays smaller than 3 ps (circles) and at 10-20 ps (triangles) depend exponentially on layer thickness.

[100] Data not shown here. Paragraph 5.2.1 discusses the occurence of the IPS upon desorption of NH_3.
[101] For 2 ML NH_3/Cu(111) the intensity of e_S was too low and the decay too fast to extract a peak shift.

The electron population dynamics are also strongly coverage-dependent, as depicted in the main panel of Fig. 5.06. The electron population decay in the late time regime slows significantly down with increasing coverage and even stops for layer thicknesses above 18 ML. Single exponential decays were fitted to the data for t < 3ps and 10-20 ps, respectively. The resulting decay times τ_{eS}^{II} and τ_{eS}^{III} as a function of NH_3 coverage are depicted in the inset of Fig. 5.06. The datasets differ from each other as the decay subsequently slows down with ongoing solvation, even on picosecond timescales. However, as apparent from the inset in Fig. 5.06, the decay times depend *exponentially* on layer thickness. The constants β = 0.24 ML^{-1} and 0.28 ML^{-1} are derived by fitting single exponentials to the data:

$$\tau(\theta) \propto \exp[\beta \cdot \theta] \tag{5.6}$$

An analysis of the early time dynamics (t < 1ps) of the different layer thicknesses, as described on the basis of Fig. 5.03, was also performed. The resulting fit parameters, localization, transition, and decay times, are depicted in Fig. 5.07 as a function of coverage. The localization time of the solvated electrons from the delocalized band to favorable sites increases from 12(5) fs to 67(5) fs with rising coverage (cf. Fig. 5.07a). However, the data scattering is so large that the localization time may also be considered to be constant with an average value of 33(7) fs for Θ < 18 ML. The initial decay time τ_{eS}^{I} (Fig. 5.07b) is for all coverages constant except of 11.5 ML. Treating this data point as an outlier, an average initial decay time of 130(60) fs results. The characteristic time for the transition from e_S^I to e_S^{II} (Fig. 5.07c) is constant for coverages above 8 ML: τ_{trans} = 180(100) fs.[103]

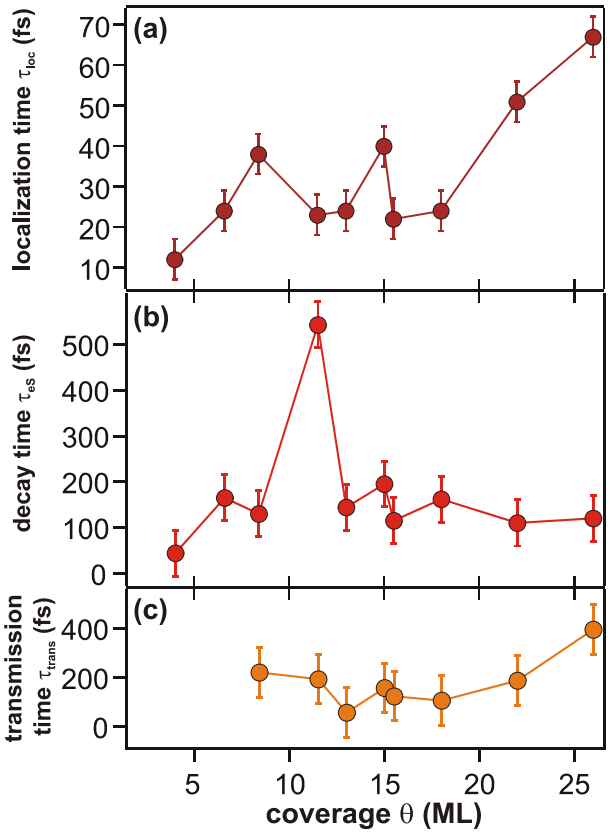

Fig. 5.07: *Early Time Dynamics.* Localization time τ_{loc} (a), decay time τ_{es}^{I} (b), and transition time τ_{trans} (c) as a function of NH_3 coverage. See text for details.

The population dynamics of solvated electrons in amorphous NH_3 layers on Cu(111) can thus be summarized as follows: In the early time regime (t < 300 fs) the transfer dynamics are barely affected by an increase of the layer

[102] This effect is *not* due to the work function change depicted in Fig. 5.05a, as the energy of e_S rises with increasing coverage: The work function first drops, then remains constant, and finally rises.

[103] The electron population decay for Θ < 8 ML is so fast, that τ_{trans} cannot be evaluated.

thickness while at late delays – where the electron decay slows significantly down – an exponential dependence of the charge transfer times on the NH_3 coverage is discerned. This exponential behavior suggests electron transfer that is mediated by tunneling through a potential barrier, which depends on the layer thickness, as tunneling probabilities depend exponentially on the barrier width. The transfer time would then be determined by (5.6), where β describes the influence of all other parameters (e.g. electron mass, barrier height) determining the tunneling probability. For such a scenario electron solvation in the surface region of the ammonia layer would be required. The left panel of Fig. 5.08a shows the situation of a thin film of NH_3 on the Cu(111) surface. The image potential is modified due to the electron trap in the adlayer and exhibits a minimum at the ammonia-vacuum interface. Tunneling through the potential barrier determines the charge transfer time τ_{CT}. In the case of a thick layer (right panel), the potential minimum lies further away from the metal substrate and the barrier is thus widened. The transfer time increases – in agreement with the experimental observation – exponentially with layer thickness.

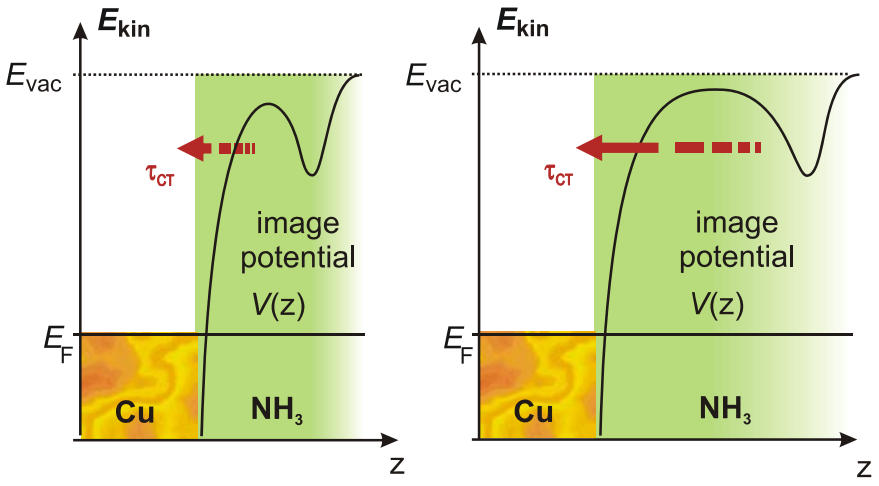

Fig. 5.08: *Charge Transfer Mediated by Tunneling.* For thin ammonia layers (left) the potential barrier between solvated electron and metal is smaller than for thick films (right). The tunneling probability decreases with increasing layer thickness.

However, at early delays, the dynamics hardly change with layer thickness. The decay time of the first isomer e_S^I is independent of layer thickness despite the strong coverage dependence of isomer e_S^{II}. Two interpretations of this observation are possible: (i) Electron solvation of isomer e_S^I occurs in the bulk of the ammonia adlayer and the transition to isomer e_S^{II} is governed by a hopping of the electron to the surface region or (ii) the charge transfer in the early time regime of isomer e_S^I is not mediated by tunneling through a potential barrier, but occurs due to strong wave function overlap with the substrate as it was the case in the substrate-dominated transfer regime of the ice-metal interfaces (cf. paragraph 4.1.1). Hence, testing the solvation site of e_S^I can show, which explanation for the different coverage dependences of the two isomers is applicable.

As discussed in 4.1.3, the surface science approach employed here offers a reliable method to determine the solvation site: A xenon overlayer experiment. Fig. 5.09a shows 2PPE spectra of 8 ML NH_3/Cu(111) at 65 fs (top) and 1 ps (bottom) before (black) and after adsorption of 2 ML xenon film. The peak maxima shift upon Xe titration by 0.20(2) eV for the early delay, i.e.

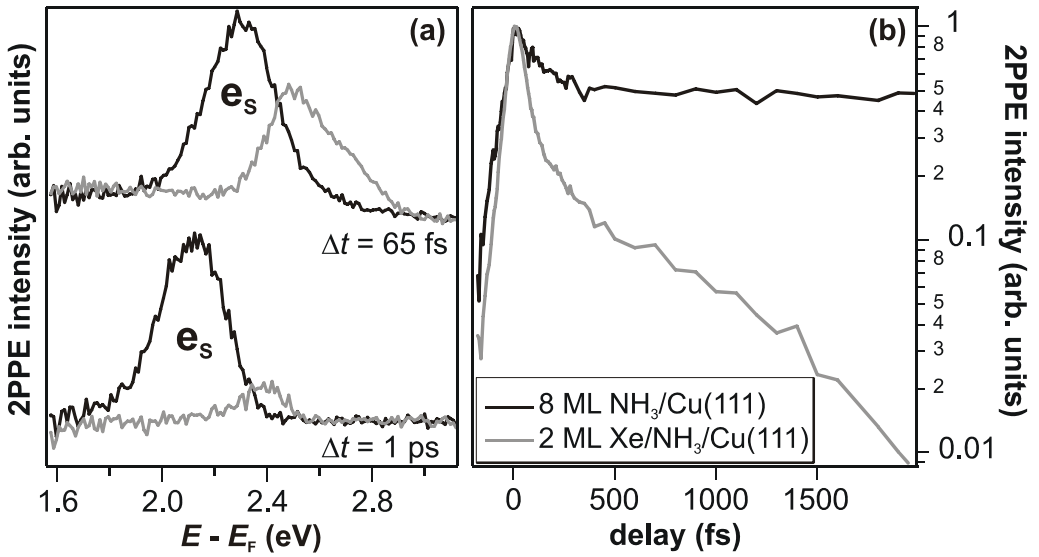

Fig. 5.09: *Xenon Overlayer Experiment.* a) For early (top) and late delays (bottom), i.e. for isomer e_S^I and e_S^{II}, the maximum of the solvated electron distribution shifts to higher energies upon Xe exposure of 2 ML. b) The electron decay is accelerated upon Xe titration.

isomer e_S^I, and 0.27(2) eV for the late time regime, i.e. isomer e_S^{II}.[104] Although this energetic shift is weaker than in the case of D_2O clusters on Cu(111) (>400 meV, see 4.1.3), it can be concluded, that both isomers, e_S^I and e_S^{II}, are localized in the surface region of the NH_3 layer.[105] The lower binding energy of excess electrons in the case of Xe/NH_3/Cu(111) compared with the NH_3/Cu(111) interface suggests a smaller degree of screening. This scenario is supported by the population dynamics of the solvated electrons shown in Fig. 5.09b. The electron decay accelerates significantly upon Xe titration. The screening of the excess electrons is reduced by the presence of the xenon layer so that their lifetime drops.

Taking into account surface solvation for both isomers of solvated electrons in ammonia layers on Cu(111), the lack of coverage dependence of the decay time of e_S^I (Fig. 5.07b), and the notable influence of layer thickness on the population decay of isomer e_S^{II}, the following scenario can be concluded: After excitation into the NH_3 adlayer, the electrons localize in the surface region. As their initial decay time τ_{eS}^I = 130 fs is unaffected by layer thickness variations within the experimental resolution, the charge transfer back to the metal substrate occurs due to finite wave function overlap with the metal. However, being localized in the surface region of the ammonia adlyer, the wave function overlap of e_S^I with the metal should vary with layer thickness, too. The complete lack of coverage dependence thus suggest, that the rate-limiting step for substrate-dominated charge transfer is *not* the amount of wave function overlap of the electron with the metal, but the electronic properties of the substrate, i.e. band gap and DOS.

[104] The shift of the peak maxima cannot result from the clearly smaller change of the sample work function of 70 meV.
[105] The weaker effect might be due to a lower charge density in the vacuum/Xe layer. Possibly, the electrons have a larger residence probabiltiy in the first NH_3 layers than the solvated electrons at the D_2O/Cu(111) interface.

The orientational band gap of Cu(111) (cf. 2.4.2) determines the transfer rate mediated by elastic and inelastic scattering. The *elastic* back transfer of the localized electron is illustrated in Fig. 5.10. The vertical (energy) and horizontal axes (parallel momentum) span the surface electronic structure of the Cu(111) template; the diagonal axis determines the distance from the NH_3/Cu(111) interface. The solvated electron is localized, i.e. it exhibits a finite width in momentum space. As electron transfer to the center of the surface Brioullin Zone is forbidden (due to the band gap) the electron has to change its momentum before it can elastically transfer to unoccupied metal states. The width (and the height in the case of inelastic decay) of the band gap determine the probability of back decay. The lack of coverage dependence for the NH_3/Cu(111) interface and the similar transfer time of the D_2O/Cu(111) system (τ_1^{Cu} = 140 fs, cf. 4.1.1) suggests that the Cu(111) band gap, and not the absolute value of wave function overlap, determines the transfer rate. This regime of ET is – in accordance with the D_2O-metal interfaces – *substrate-dominated*.

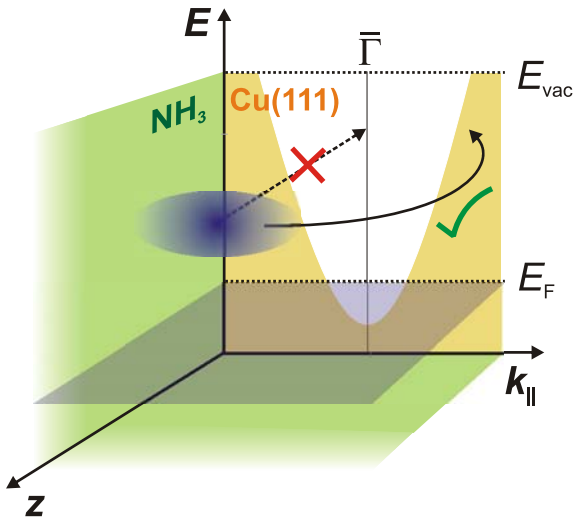

Fig. 5.10: *Elastic Electron Scattering.* Electron decay is determined by the orientational sp-band gap of the substrate, which allows elastic back transfer only in parallel with a momentum change of the electron.

The transition to the second isomer, e_S^{II}, occurs within 180 fs. The electron decay from e_S^{II} exhibits an exponential dependence on coverage and is thus mediated by tunneling. ET in this late time regime (t > 300 fs) is therefore – as in the ice-metal case – *barrier-determined*, i.e. mediated by tunneling through a potential barrier at the NH_3/Cu(111) interface. However, in contrast to the ice adlayers, where the electrons were localized in the bulk of the D_2O layer (i.e. at a fixed distance from the metal), the barrier between the surface-solvated electrons and the substrate changes at the ammonia-Cu(111) interface with layer thickness, leading to coverage-dependent ET times.

Having revealed the processes of charge injection, localization, and back transfer for the ammonia-Cu(111) system, investigation of the *coupling degree* of the solvated electrons to the copper substrate is required. The next paragraph presents temperature-dependent measurements of amorphous multilayers NH_3/Cu(111), showing that charge transfer occurs thermally activated.

5.1.3 Tuning the Coupling Degree

Fig. 5.11a presents the solvated electron population traces of a 12 ML film of NH_3/Cu(111) as a function of sample temperature. Note that the time axis is in logarithmic scale to ensure recognition of the dynamics on all timescales. The different traces between 28 and 62 K exhibit varying dynamics: At low sample temperatures the solvated electron resides for hundreds of picoseconds in the adlayer, while their lifetime reduces to few hundred femtoseconds for $T >$ 60 K. To assure that this change of electron decay rate is due to the temperature increase and *not* because of structural changes induced by temperature, the following test experiment was performed: The NH_3-covered sample was heated to the respective temperatures and annealed for two minutes until the 2PPE signal stabilized. Subsequently, the system was cooled down to carry out the 2PPE measurement at 28 K. The resulting population traces are depicted in Fig. 5.11b. Apparently, the annealing does not have any influence on the electron dynamics up to 55 K; even heating to 62 K leads to only slight changes of the decay rate.

To quantify the influence of temperature on the electron population dynamics, the three-level rate equation model derived in paragraph 5.1.1 was fitted to the data up to 3 ps as shown by the red curves in Fig. 5.11. At larger delays the population decay slows increasingly down due to the increasing screening of the excess electrons by the solvent molecules. The characteristic times resulting from the three-level fit are plotted in Fig. 5.12 as a function of sample temperature. Transition (yellow) and localization time (red) remain constant within the experimental resolution. The decay time of isomer e_S^I (orange) is hardly affected by the sample temperature and drops only slightly with ~3(1) fs/K (dashed line in panel (a)). Fig. 5.12b depicts the transfer time τ_{eS}^{II} of isomer e_S^{II}, which significantly changes upon heating. The

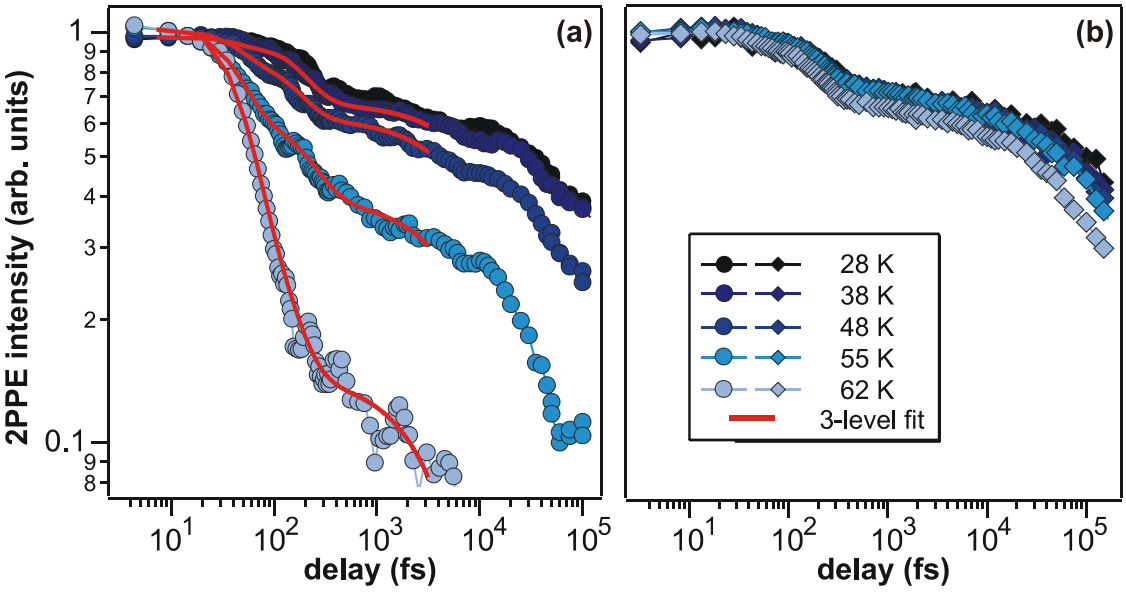

Fig. 5.11: *Temperature Dependence of Electron Population Dynamics for 12 ML NH_3/Cu(111).* a) The electron decay accelerates significantly with increasing temperature. This effect is not induced by structural changes: b) XC traces for annealed ammonia layers, measured at 28 K. Up to 62 K hardly any structural effect is observed.

transfer rate $\Gamma_{eS}^{II} = (\tau_{eS}^{II})^{-1}$ is shown in Fig. 5.12c (light blue markers) as a function of the inverse temperature (Arrhenius Plot). In addition also the decay rate at late delays for $t > 13$ ps, achieved by fitting a single exponential to the data of Fig. 5.11, is depicted in Fig. 5.12c (dark blue diamonds). Thermally activated charge transfer is supposed to follow the Arrhenius Function:

$$\Gamma(T) = a \cdot \exp\left[-\frac{E_a}{k_B T}\right] + \Gamma_0 \tag{5.7}$$

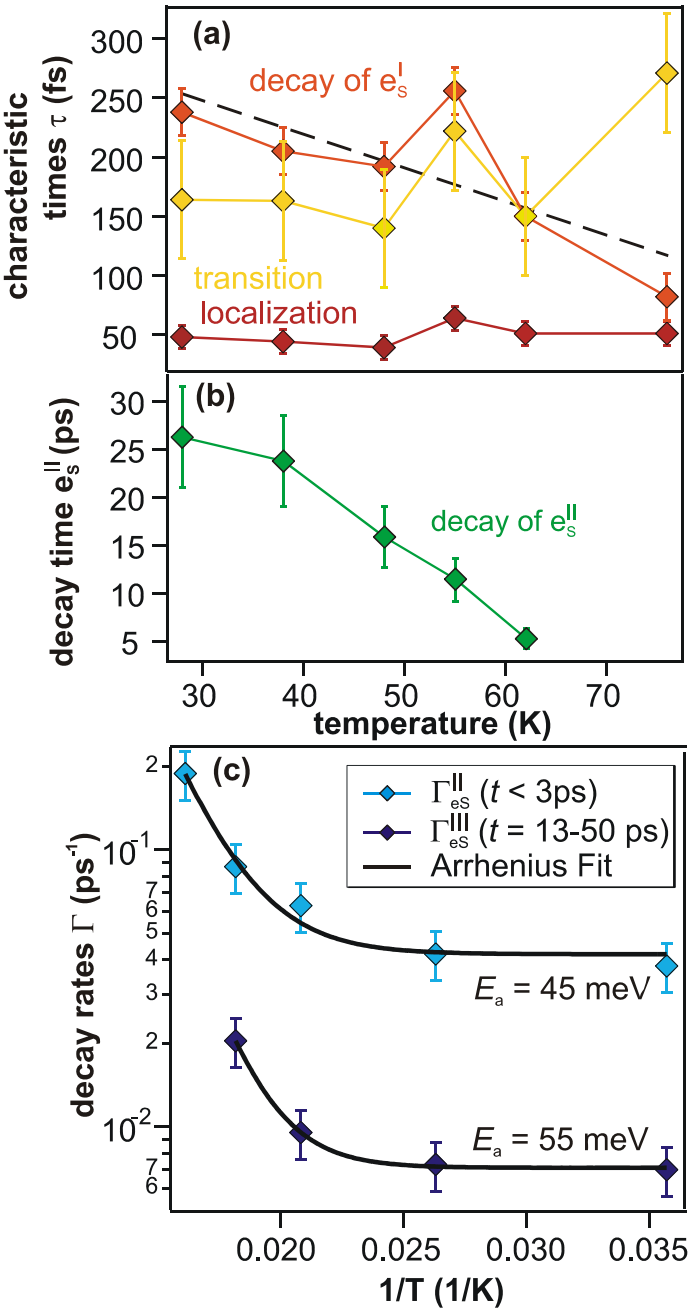

Fig. 5.12: *Temperature Dependence of Characteristic Times and Rates.* a) The localization (red), transition (yellow), and decay time of e_S^I (orange) are almost unaffected by changes of the sample temperature. b) The initial decay time of isomer e_S^{II} decreases significantly with temperature. c) Arrhenius Plot of the initial (t < 3 ps, light blue) and the late decay rate (13-50 ps, dark blue) of isomer e_S^{II}. Black curves are least square fits to the data on the basis of equation (5.7).

The least square fits based on equation (5.7) are presented by the black curves in Fig. 5.12c. The temperature-dependent change of charge transfer rates is excellently reproduced. The two datasets, Γ_{eS}^{II} and Γ_{eS}^{III}, present activation barriers of E_a = 45(7) meV and 55(9) meV, respectively. Furthermore, the transfer rates for T = 0 K results from the least square fits: Γ_0 describes the tunneling probability to the metal substrate *without* thermal assistance. With 24(5) ps (for t < 3 ps) and 140(30) ps (for t = 13-50 ps) this threshold transfer time increases with increasing time delay, i.e. degree of solvation. This is noteworthy, as it shows that the better the screening of the excess electron at late delays leads to a weaker coupling (smaller Γ_0) *and* to a higher nuclear barrier that has to be overcome for thermally activated electron decay. Having in mind that ET occurs for isomer e_S^{II} via tunneling to the substrate, it can be concluded that thermally assisted tunneling is observed for the NH_3/Cu(111) system in contrast to the amorphous ice-metal interfaces investigated (cf. 4.1.4). The transfer dynamics of isomer e_S^{I}, however, are barely affected by changes of the sample temperatures. Accordingly, electrons in isomer e_S^{I} are considerably stronger coupled to the substrate than isomer e_S^{II} electrons. In other words, the transition from isomer e_S^{I} to e_S^{II} is accompanied by a cross-over to the weak coupling limit of charge transfer.

Paragraph 5.1.2 showed that the electron transfer dynamics of isomer e_S^{II} depend on the NH_3 layer thickness, which determines the width of the interfacial tunneling barrier and therefore the coupling strength. As the occurrence of a temperature dependence of the charge transfer times apparently depends on the degree of coupling of the excess electrons to the substrate states, the thermally activated electron transfer at the 12 ML NH_3/Cu(111) interface could be different for other layer thicknesses. Fig. 5.13 presents electron population traces of an 8 ML film of NH_3 on Cu(111) at three different sample temperatures. Note again the logarithmic time axis. Apparently, the decay of solvated electrons in this thinner film is hardly affected by a temperature increase from 30 to 50 K in contrast to the 12 ML coverage (Fig. 5.11), where the transfer time decreased significantly in this temperature range.

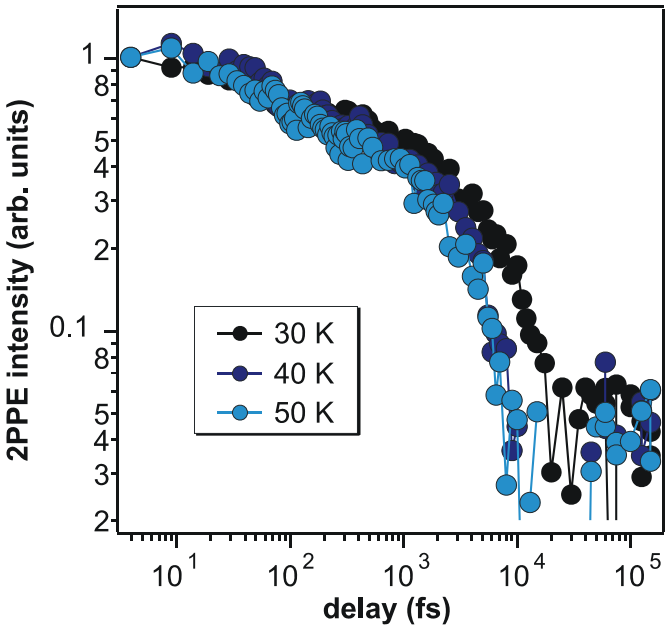

Fig. 5.13: *Temperature Dependence of Population Dynamics for 8 ML NH_3/Cu(111).* Electron population traces for four different sample temperatures. Heating to 50 K hardly affects the electron dynamics in contrast to the thick film discussed before. For T > 70 K a structural transition occurs that leads to a change of transfer rates (cf. 5.2).

The stronger coupling of solvated electrons at the surface of the 8 ML NH_3 film inhibits observation of temperature-dependent charge transfer.

The probability of electron decay via resonant tunneling through the interfacial barrier is significantly more probable than thermal fluctuations mediating transfer at higher energies. However, for higher NH_3 coverages thermally activated tunneling is observed, showing that the NH_3/Cu(111) interface offers – due to the coverage-dependent, long-living character of the excess electrons – the opportunity to *tune* the coupling degree of the solvated electrons to the metal substrate. In other words, the NH_3/Cu(111) system allows not only for the investigation of the transition between the strong and weak electronic coupling limit in real time, but also enables *adjustment* of the degree of coupling by choosing the layer thickness.

The above results of the electron dynamics at the NH_3/Cu(111) interface are useful to gain deeper understanding of the fundamental processes of charge transfer and solvation dynamics at molecule-metal interfaces. In addition, combination and comparison to the results on the dynamics at the amorphous D_2O-metal interfaces yields information of the adsorbate influence on the transfer and solvation dynamics and the underlying elementary mechanisms. Therefore, the next paragraph discusses similarities and differences of both investigated systems and develops a consistent picture of electron transfer and solvation at amorphous molecule-metal interfaces.

5.1.4 Discussion: Water vs. Ammonia

For all investigated interfaces (amorphous D_2O/Ru(001), D_2O/Cu(111), and NH_3/Cu(111)) the charge injection of excited metal electrons into the adsorbate layer occurred non-resonantly via the conduction band of the adsorbate layer. The electrons subsequently localized at favorable sites near the bottom of this delocalized band and were stabilized by a reorientation of the surrounding polar solvent molecules leading to an increase of the excess electron's binding energy. In all cases, the initial binding energy with respect to the respective vacuum levels was ~1 eV. However, the succeeding solvation and transfer dynamics differed significantly.

Solvation Dynamics: Fig. 5.14a shows the shift of the peak maximum of the solvated electron distributions of multilayer coverages of D_2O on Cu(111) (diamonds) and Ru(001) (circles) *and*, exemplarily, of 8.5 ML NH_3/Cu(111) (triangles). The two D_2O datasets exhibit different peak shifts due to the energy dependence of the electron transfer time as discussed in 4.1.1. A model calculation showed that the actual *stabilization* rates of the two systems are similar. The peak *shift*, in contrast, differs due to faster electron decay at higher energies. Fig. 5.14b illustrates the electron solvation dynamics at ice-metal interfaces: An interfacial barrier evolves and increases *steadily* with ongoing solvation (red arrow).

The electron dynamics are different for the amorphous NH_3/Cu(111) interface. The peak maximum shifts initially with a rate of -0.8 eV/ps, which becomes considerably slower for $t >$ 300 fs. As introduced in section 5.1.1, these differing dynamics correspond to two different isomers of solvated electrons, e_S^I and e_S^{II}, for early and late delays, respectively. The electrons in isomer e_S^I solvate faster compared with the electron *hydration*. Apparently, the reaction of the solvent molecules to the excess charge differs for ice and ammonia. This effect is well-

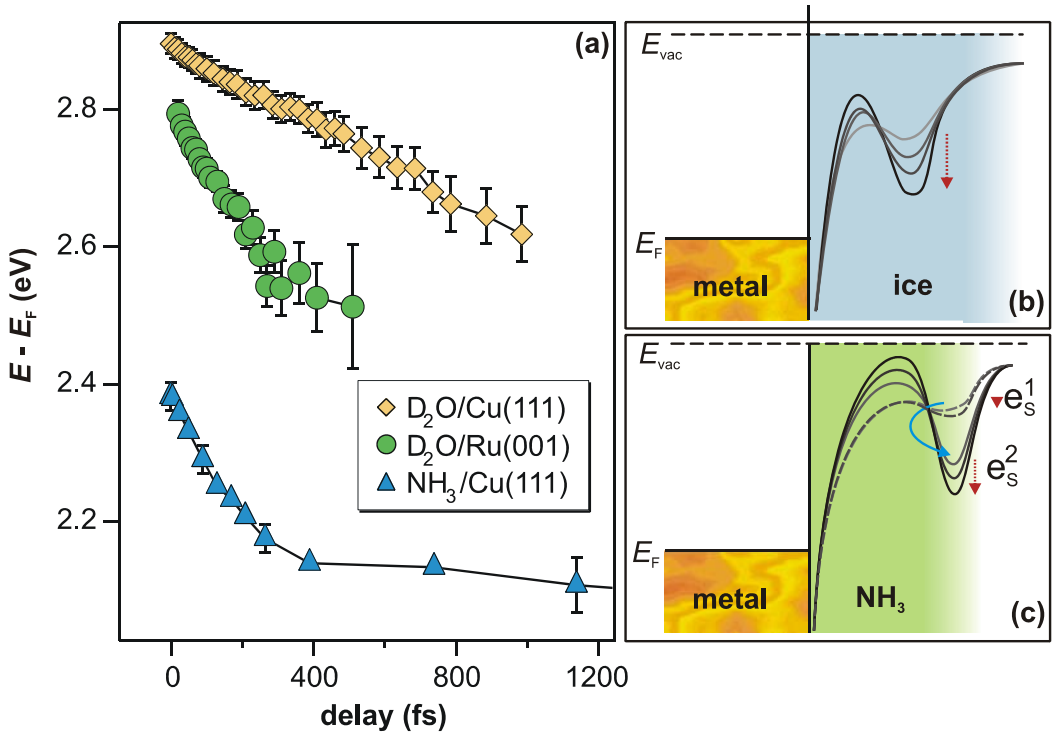

Fig. 5.14: *Electron Solvation in Ice and Ammonia Layers.* a) Peak shift for all investigated systems. b) Electron solvation in D_2O layers on metal surfaces occurs steadily, while c) the NH_3/Cu(111) system exhibits a sudden change of stabilization dynamics.

explained by the surplus of unbound hydrogens in the case of NH_3: As discussed in paragraph 2.4.1, the ammonia molecule may donate three protons for hydrogen-bonding, but only accepts one H-bond. Hence, the large amount of non-bridged hydrogen atoms may cause the faster ammoniation.

The transition from e_S^I to e_S^{II} occurs, as shown in paragraph 5.1.2, with a time constant of τ_{trans} = 180(100) fs.[106] The isomer e_S^{II} exhibits with ~10 meV/ps a considerably slower peak shift. Fig. 5.14c illustrates the electron solvation dynamics at the NH_3/Cu(111) interface: Stabilization of the excess charge starts in e_S^I. However, with the time constant τ_{trans}, the electrons pass over to isomer e_S^{II} (blue arrow) and are further stabilized. Possible explanations for this transition are (i) proton transfer directed to the solvation site which occurs on comparable timescales in NH_3 clusters, [Sny97] (ii) a reorientation of ammonia molecules mediated by the umbrella mode (ν^{-1}= 40 fs, [Sny97]), or (iii) breakage of hydrogen bonds, which are weaker in solid ammonia than in ice. However, the underlying mechanism obviously results in an enhanced screening of the excess charge, which leads to a slowing down of the stabilization dynamics.

[106] Averaged value for all layer thicknesses.

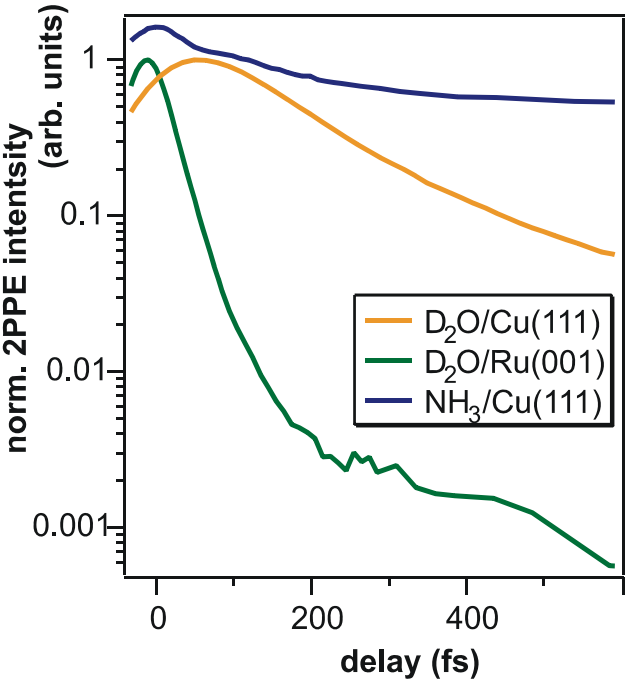

Fig. 5.15: *Electron Population Decay at Ice- and Ammonia-Metal Interfaces.* Top: In the case of D_2O on Cu(111) and Ru(001) a significant fraction of the e_S population decays within the first ps. Bottom: Initial dynamics of the solvated electron population in NH_3 layers on Cu(111).

Transfer Dynamics: Fig. 5.15 presents population traces of solvated electrons in D_2O layers on Cu(111) (orange), Ru(001) (green), and in 8.5 ML amorphous ammonia on Cu(111) (blue). In the case of the *ice* adlayers the excess electrons decay to the respective substrates within the depicted time range (top panel), while a significant fraction of the solvated electrons at the NH_3/Cu(111) interface remains in the adlayer (bottom panel). It was shown in paragraph 4.1.1 by an empirical model calculation that the electron back transfer from an amorphous ice layer to the metal can be separated into two different regimes, the *substrate-dominated* and the *barrier-determined* transfer regime. At early delays (t < 300 fs) the electron decay is determined by the substrate's electronic surface band structure, while at late delays (t > 300 fs) an increasing interfacial barrier becomes the rate-limiting step for charge transfer, which is mediated by tunneling.

For ammonia on Cu(111) two isomers of solvated electrons were found (cf. 5.1.1). It could be shown by coverage-dependent measurements that the transfer time of the isomer e_S^I in the early time regime (t < 300 fs) is independent of the layer thickness, while the decay time of the second isomer e_S^{II} depends exponentially on coverage. Being localized in the surface region of the NH_3 layer (cf. 5.1.2), electrons in e_S^{II} decay via tunneling through an interfacial barrier; the charge transfer is *barrier-determined*. The back transfer of isomer e_S^I is different due to its finite wave function overlap with metal states. It experiences the substrates electronic band structure including the orientational sp-band gap of Cu(111). As in the case of ice-metal interfaces, the charge transfer probability is determined by the rates for elastic and inelastic scattering to the substrate. The electron transfer is *substrate-dominated*.

Besides these similarities of the investigated systems, one major difference discriminates the NH_3/Cu(111) from the ice-metal interfaces: The transition from e_S^I to e_S^{II} is governed by a sudden deceleration of electron transfer dynamics. The long-living character of the ammoniated electrons enables the observation of *temperature-dependent* charge transfer. As discussed in paragraph 4.1.4, a comparable behavior was not found for the amorphous ice-metal interfaces. Fig. 5.16 illustrates the course of events of solvation at the 12 ML NH_3/Cu(111) interface with the aid of the two-dimensional potential energy surface for heterogeneous electron transfer,

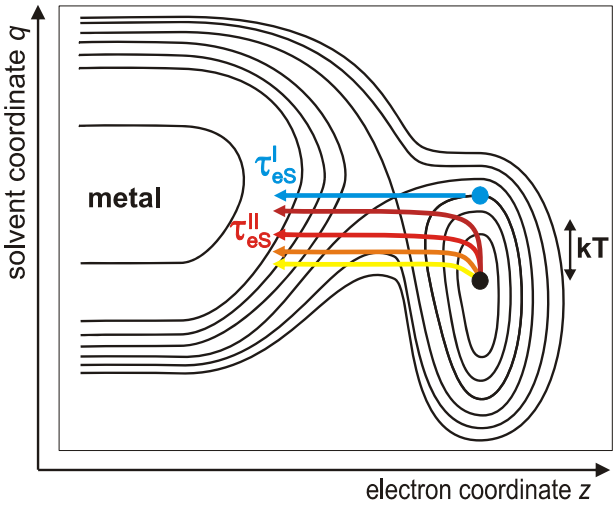

Fig. 5.16: *ET at the NH_3/Cu(111) Interface.* In the early stages of solvation the electronic coupling between excess electron and metal is so strong that charge transfer is (nearly) temperature-independent (blue). Being weakly coupled at late delays, ET is mediated by thermal fluctuations of the solvent.

which is spanned by the real space coordinate x and the solvent coordinate q. Electrons of isomer e_S^I (blue) are still strongly coupled to the substrate and decay with a nearly temperature-independent rate back to the metal. However, e_S^{II} electrons (black) are only very weakly coupled to the Cu(111) template. They transfer by thermally activated solvent rearrangement to the metal and their transfer time τ_{eS}^{II} decreases with increasing temperature (yellow and red arrows). Activation barriers of ~50 meV were determined for this charge transfer, which is accordingly termed thermally assisted tunneling. The extrapolated ET times for $T = 0$ K of 24 ps (for $t < 3$ ps) and 140 ps (for $t = 13$-50 ps) are a measure for the bare coupling degree of the ammoniated electrons to the Cu(111) substrate.

Conclusions

The charge injection, localization, solvation, and back transfer of amorphous ice- and ammonia-metal interfaces have been investigated by time-resolved 2PPE spectroscopy, allowing for detailed understanding of the underlying fundamental processes. Electrons are injected into the adlayers via the respective conduction band and localize due to fluctuations in the modified image state potential. The electric field of the excess charge causes a rearrangement of the surrounding polar molecules resulting in an energetic stabilization of the electron. The faster stabilization in NH_3 layers (compared with ice), which is probably due to the high number of unbound protons, leads to a stronger decoupling from the substrate than for the ice-metal interfaces. A sudden deceleration of the solvation and transfer dynamics is observed. This abrupt change is attributed to a momentous change of the ammonia configuration, which leads to a sudden increase of screening. The resulting smaller net electric field of the excess electron leads to a deceleration of the solvation dynamics. Furthermore, the resulting long lifetimes enable investigation of charge transfer dynamics in the weak coupling limit.

The comparison of ice- and ammonia-metal interfaces finally lead to a better understanding of the dynamics of HET: Being strongly coupled to the respective substrate, thermal fluctuations of the solvent do not influence the electron transfer from an amorphous *ice* adlayer. The electrons at the ice-metal interfaces decay by tunneling (blue arrow in Fig. 5.16), before they are sufficiently decoupled from the metal to observe thermally activated transfer dynamics. The ET from an *ammonia* adlayer to the Cu(111) substrate however reaches the weak coupling limit, as excess electrons are – depending on coverage – increasingly decoupled from the metal. This weak coupling to the metal enables observation of thermally activated tunneling (cf. red and orange arrows in Fig. 5.16). A solvent fluctuation (i.e. change of q) enhances the transfer probability. Furthermore, the higher degree of coupling in the early stages of electron solvation (t < 300 fs) leads to (nearly) temperature-independent ET. Thus, the ammoniated electron allowed for the observation of the transition between the strong (Landauer) and weak (Marcus) coupling limit. In other words, it was shown that both coordinates, real space z and solvent q, have to be considered when drawing a complete picture for electron transfer at molecule-metal interfaces.

5.2 Ultrafast and Ultraslow Dynamics in Crystalline Ammonia

The present section presents the changes of electron solvation and transfer dynamics induced by the crystallization of the ammonia adlayers, showing that the new structure leads to the formation of an image potential state at the interface (5.2.1) and modification of the sample work function. In addition, similar to the ice-metal interfaces, also electron solvation is strongly affected by the structural transition: Ultralong-living electrons are found, exhibiting lifetimes on the order of minutes and a notable temperature dependence (5.2.2). However, lifetimes and stabilization dynamics differ compared with the electron dynamics at crystalline ice-metal interfaces as discussed in paragraph 5.2.3.

5.2.1 Transition to the Well-Ordered Phase: IPS

The top panel of Fig. 5.17 presents the 2PPE intensity of a 5 ML NH_3 film on Cu(111) as a function of sample temperature (bottom axis) and intermediate state energy (left axis) with respect to the Fermi Level E_F in false color representation. In parallel to 2PPE, the NH_3 desorption yield was monitored by the QMS: As depicted in the bottom panel of Fig. 5.17, multilayer desorption starts at ~90 K.[107] Note that, as the coverage decreases with increasing

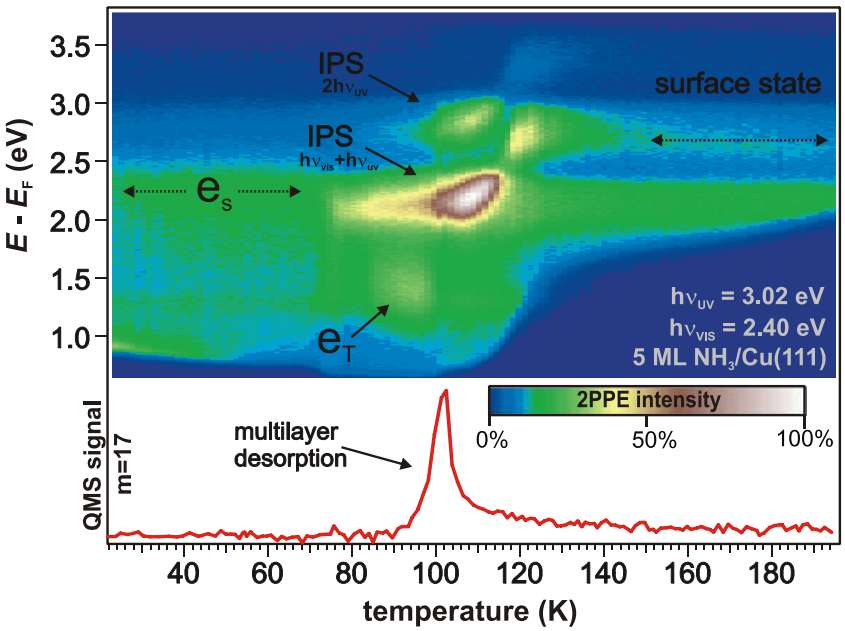

Fig. 5.17: *Temperature 2PPE and TD Spectroscopy.* Top: 2PPE intensity in false color representation as a function of temperature and energy (at t = 0 fs). At 80 K the IPS of the interface evolves. In parallel trapped electrons e_T occur at lower energies. After multilayer desorption (T > 110 K) the Cu(111) surface state appears at 2.6 eV. Bottom: Thermal desorption yield of NH_3 during sample heating.

[107] The 2nd and 1st monolayer desorption substructures are not resolved in this TDS as the sample was situated in the TOF spectrometer during measurement, which reduces resolution. The measurement was done with a heating rate of 0.3 K/s.

temperature, the 2PPE spectra shown in the top panel are a result of both, the temperature and the coverage variation.

The 2PPE spectra for $T < 70$ K exhibit two features. The peak at 2.4 eV results from the solvated electrons e_S discussed in the previous section. The abrupt intensity change at 0.9 eV, the low-energy cut-off, is attributed to the secondary edge. As apparent from Fig. 5.17, it changes significantly upon heating and NH_3 desorption. The secondary edge can be used to determine the sample work function, when plotted versus final state energy, as introduced in 3.4.1. As temperature and coverage influence on the work function cannot be separated, Fig. 5.18 depicts the evaluated work function (green diamonds) as a function of sample temperature *and* NH_3 coverage in panel (a) and (b), respectively. It drops upon heating from 3.29(2) eV (T = 25 K) to 3.08(2) eV at 90 K (Fig. 5.17a). In this regime a coverage dependence can be excluded as desorption starts at higher temperatures. This decrease is probably due to a rearrangement of the ammonia dipoles accompanying the transition from the metastable amorphous to the well-ordered phase and is in good agreement with the literature value of 2.95(10) eV. [Her95] During multilayer desorption ($\Theta > 2$ ML, cf. Fig. 5.18b), the work function rises only slightly. However, at even higher temperatures ($T > 108$ K), when desorption of the second monolayer *occurs*, the work function increases significantly. As apparent from Fig. 5.18b this increase starts at a coverage of 2 ML and continues to 4.02(10) eV until the second monolayer has desorbed completely. This work function value does not agree with the literature value of 3.3(1) eV of Hertel *et al.* measured at 100 K. [Her95] This discrepancy could be explained by the higher temperature in the present experiment: (> 130 K). A higher mobility of the NH_3 molecules on the surface might lead to the higher global work function compared with Hertel's work. However, the desorption of the first monolayer, finally, is governed by a work function increase up to the Cu(111) value of 4.95 eV.

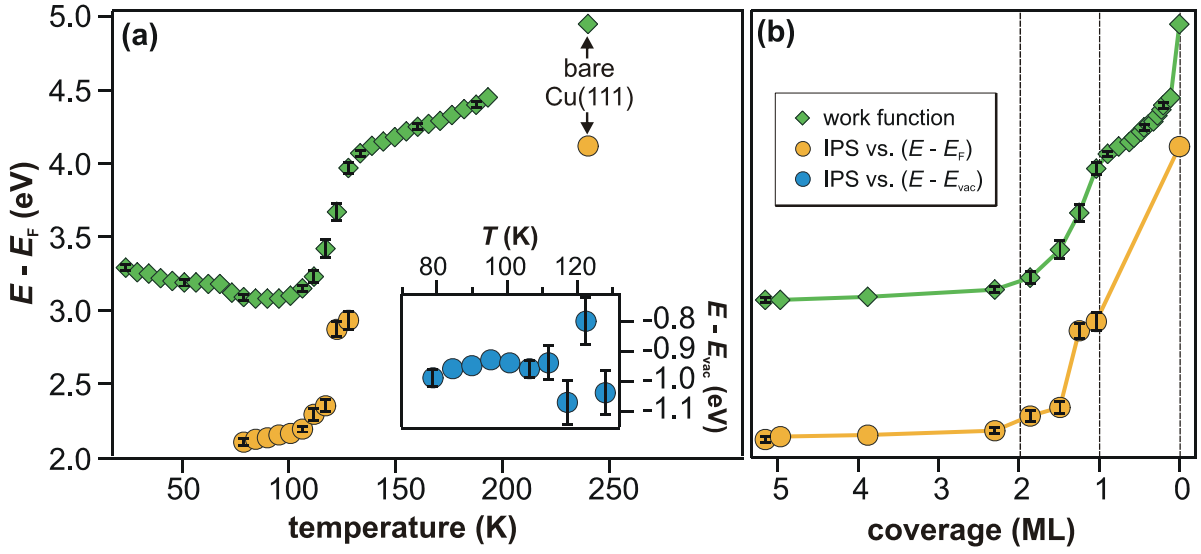

Fig. 5.18: *Work Function and IPS of NH_3/Cu(111).* a) Work function and IPS intermediate state energy as a function of sample temperature. Inset: The binding energy of the IPS with respect to E_{vac} is constant. b) Coverage dependence of IPS and work function change.

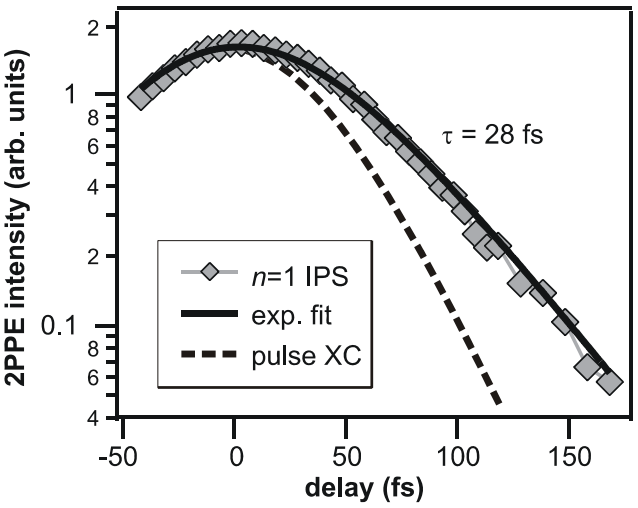

Fig. 5.19: *Population Dynamics of the IPS.*

In addition to the temperature/ coverage dependence of the sample work function Fig. 5.17 reveals the occurrence of new 2PPE features for $T > 80$ K: A peak evolves at 2.1 eV, which reaches maximum intensity at 100K. Its maximum shifts with increasing temperature and decreasing layer thickness to higher energies as shown by the orange circles in Fig. 5.18. In fact, it follows the evolution of the sample work function as apparent from the inset in Fig. 5.18a: The binding energy with respect to the sample's vacuum level E_{vac} remains constant and is comparable to the one of the $n = 1$ image potential state of the bare Cu(111) surface of -0.83 eV. [Fau95] Having in mind that a structural transition of the NH_3 adlayer occurs at ~100 K (cf. 3.3.2), it is concluded – in accordance with similar observations at D_2O-metal interfaces [Gah04] – that this feature results from the $n = 1$ IPS of the NH_3/Cu(111) interface that appears upon the crystallization of the ammonia adlayer. As apparent from Fig. 5.17, the spectral signature occurs twice in the data: Due to electrons that are pumped *and* probed by UV photons (in contrast to the UV-VIS pulse sequence), a "second" IPS peak lies at energies higher than the "first" by $\Delta h\nu = 0.6$ eV. Fig. 5.19 depicts the population dynamics of the IPS (markers). The black curve is the least square fit of a single exponential decay convolved with the laser pulses cross correlation (dashed curve) revealing the lifetime of 28(5) fs of electrons in the IPS.

Two more features evolve during heating in Fig. 5.17: After the desorption of the multilayer ($T > 110$ K) the occupied surface state of the bare Cu(111) surface appears in the spectra at 2.6 eV (initial state energy: $E - E_F = -0.4$ eV). However, in parallel with the occurrence of the IPS, another feature appears at energies below 1.5 eV. It is attributed in the next paragraph to trapped electrons e_T in the ammonia adlayer exhibiting lifetimes on minute timescales and a comparable temperature dependence as the ultralong-living electrons in crystalline ice presented in 4.2.

In conclusion, NH_3/Cu(111) exhibits – as D_2O on metal surfaces – a transition from an amorphous to the crystalline phase during multilayer desorption. In parallel with crystallization an IPS is observed at the interface, which is a common attribute of a well-ordered surface. In addition, a new spectral feature, e_T, evolves, which subsequently disappears with multilayer desorption.

5.2.2 Freezing Hot Electrons in Crystalline Ammonia

The ultralong-living character of the peak e_T becomes apparent by Fig. 5.20. The figure shows exemplarily a pump-probe experiment at 5 s time delay between UV and VIS laser pulse of a 3 ML film of crystalline NH_3/Cu(111) in false color representation. The left panel depicts the time evolution of the e_T feature (1.65(3) eV intermediate state energy), which is pumped and probed by UV photons. The bottom panel depicts the macroscopic time evolution of the spectral feature, integrated over the energy interval indicated by the blue rectangle. As the 2PPE intensity of the peak rises on this macroscopic timescale (seconds), it is concluded that – similar to D_2O/Ru(001) (cf. 4.2.1) – irradiation of the sample leads to a photostationary state resulting from the competition of electron excitation and depopulation by the UV light. According to the exponential fit (black curve) equilibrium is reached with a time constant of 0.25(10) s. Consequently, the trapped electrons are on average 0.25 s "old". The sample was irradiated with UV photons for 5 s and left in darkness for the desired time delay (here 5 s). Then, as depicted in the left panel of Fig. 5.20, the trapped electron population was probed using VIS light (intermediate state energy on the right axis). As apparent from the intensity trace (orange diamonds)[108] the electrons are still trapped in the ammonia layer and depopulated very efficiently by the visible photons: The main part of the electron population of e_T is probed within the first time step of Δt = 0.2 s.[109]

Similar experiments have been performed for a series of different time delays up to 120 s. The resulting 2PPE spectra of trapped electrons in crystalline ammonia on Cu(111) are presented in Fig. 5.21 as a function of intermediate state energy (bottom axis) and time delay (right axis).[110] The peak maximum of the solvated electron distribution shifts to lower

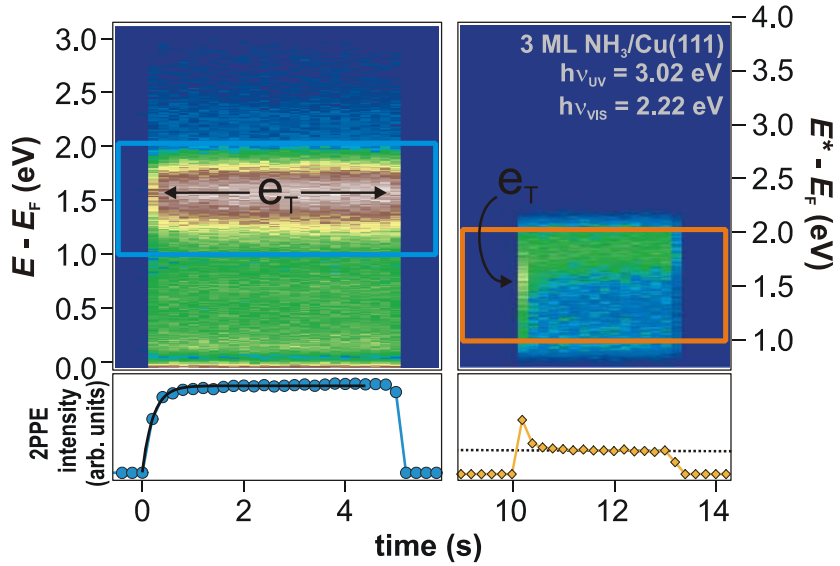

Fig. 5.20: *Pump-Probe Experiment on Macroscopic Timescales.* Left: The sample is irradiated by UV light for 5 s until the photostationary state is reached. The bottom panel depicts the intensity evolution (blue markers). The exponential fit (black curve) results in a rise time of 0.25 s. Right: After 5 s of darkness the trapped electron population is probed by VIS light and efficiently depopulated as apparent from the intensity trace at the bottom (orange markers). The dotted line indicates the constant background.

[108] Integration over the energy interval indicated by the orange rectangle in the top panel.
[109] The constant intensity for t > 10.5 s is due to the constant background of the 2PPE spectra.
[110] The spectrum at 0.25 s was extracted from the left panel in Fig. 5.20.

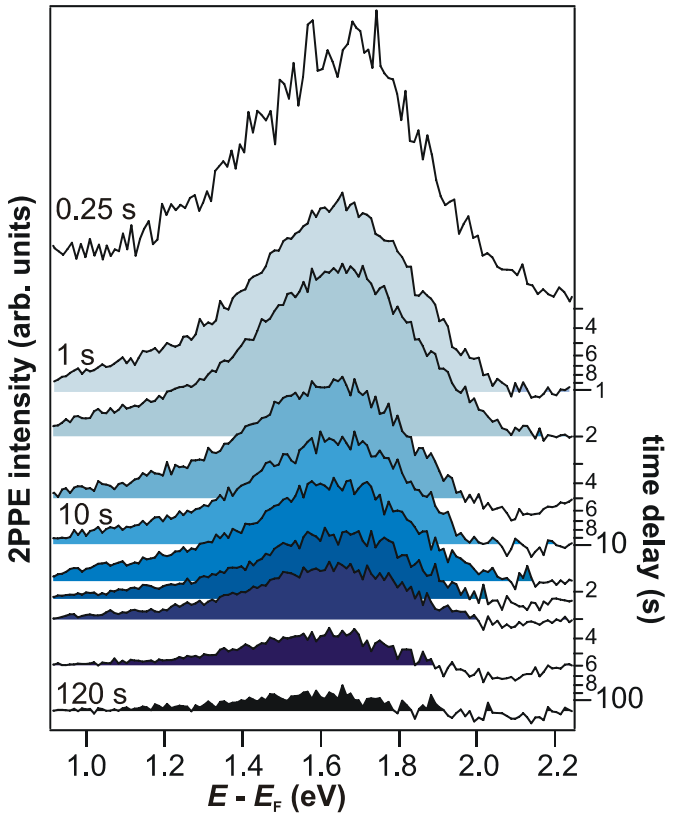

Fig. 5.21: *Time-Resolved 2PPE Spectra of Crystalline NH_3/Cu(111).* Trapped electrons in crystalline ammonia exhibit dynamics on the timescale of minutes. After 120 s most intensity has decayed. The peak maximum of the solvated electron distribution shifts down to lower energies with increasing time delay. See text for details.

intermediate state energies with increasing time delay and its intensity decreases. After 120 s the main part of the trapped electron population has decayed. The shift of the peak maximum is depicted in Fig. 5.22 as a function of time delay (logarithmic scale). Starting at 1.65 eV (t = 0.25 s), the trapped electrons reach a binding energy of 1.58(4) eV above E_F after two minutes.

Apparently, crystalline ammonia layers exhibit comparable electron dynamics as crystalline ice. Electrons are injected into the ammonia adlayer and are so efficiently screened from the metal substrate that they exhibit lifetimes up to minutes more than 1 eV above the Fermi Level. Before turning to a detailed comparison of the trapped electron *dynamics* in crystalline ammonia and ice in paragraph 5.2.3, the second characteristic of these ultralong-living electrons is investigated: Fig. 5.23 depicts the energetic shift of the e_T peak maximum as a function of sample *temperature*. Heating the sample from 28 K to 100 K leads to a gain in binding energy that is larger than 300 meV. It is not possible to

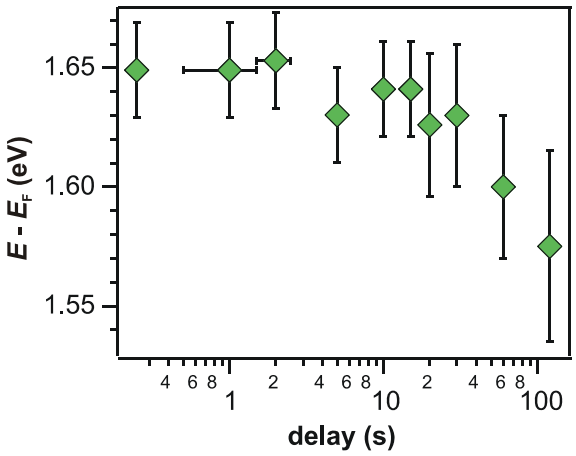

Fig. 5.22: *Time-Dependent Peak Shift of e_T.*

extract the peak position for higher temperatures as multilayer desorption starts and the spectral signature of the trapped electrons disappears (cf. Fig. 5.17). Trapping of ultralong-living electrons is apparently not possible for coverages below 2 ML.

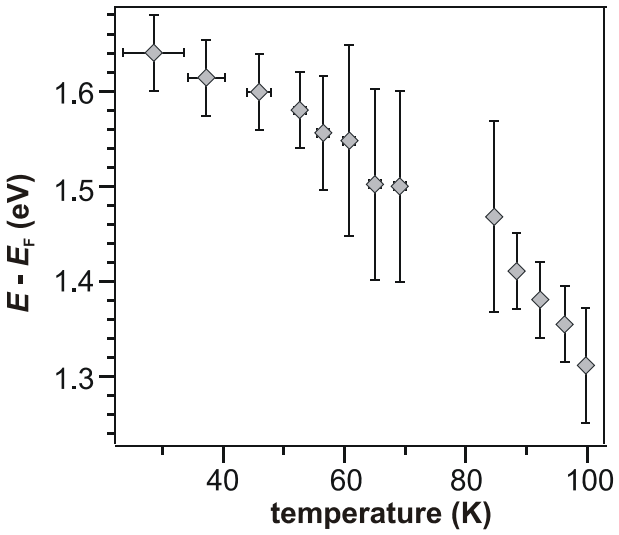

Fig. 5.23: *Temperature-Dependent Peak Shift of Trapped Electrons.* The peak maximum of the solvated electron distribution approaches the Fermi Level with increasing temperature.

On the basis of the above observations, it can be concluded that – similar to ice-metal interfaces – ultralong-living, trapped electrons are observed in crystalline ammonia layers in front of the Cu(111) surface. The extremely long lifetime of these excess electrons (on the timescale of minutes) despite their intermediate state energy of more than 1 eV above the metal's Fermi Level and their pronounced temperature dependence is remarkable. Furthermore, it is noteworthy that the observation of such an exceptional spectral feature with enormous lifetime and significant temperature dependence as the trapped electrons in crystalline ice could also be observed for the NH_3/Cu(111) system and not only for the D_2O/Ru(001) interface. The appearance of ultralong-living electrons in a different solvent than ice is highly important, as this finding shows that they are *not* a specific characteristic of ice, but might be of general importance for more polar solvents. The next paragraph compares the attributes of trapped electrons in crystalline ammonia with the results of the ice-metal interfaces (cf. section 4.2) and discusses similarities and differences of the two adsorbates.

5.2.3 Discussion: Electron Trapping in Crystalline Solvents

Electron trapping has been observed for crystalline ice *and* ammonia adlayers on metal surfaces. Excess electron lifetimes on the order of minutes have been found for both investigated systems, despite intermediate state energies several eV above Fermi Level of the respective substrate. For the ice-metal interface a stretched exponential model was developed to handle the electron dynamics ranging over 17 orders of magnitude in time. As – in addition – temperature-dependent measurements showed that electron stabilization occurs thermally activated, the stretched exponential approach was supplemented by the introduction of conformational substates (CSS), over which electron solvation proceeds. It was shown, that progression along the electron solvation coordinate q occurs due to thermally activated reorientation ("flips") of D_2O molecules at the surface of the adlayer. Having observed similar, ultralong-living electrons for the NH_3/Cu(111) system, quantitative comparison of time- and temperature dynamics can yield deeper insight into the underlying processes.

Fig. 5.24a depicts the temporal peak shift of the trapped electron distribution in crystalline D_2O (orange circles) and NH_3 layers (green diamonds) on Ru(001) and Cu(111), respectively. As the intermediate state energy of e_T differs for ice and ammonia, different energy axes (NH_3: left, D_2O: right) were employed to compare the bare *dynamics*, i.e. *change* of peak position with time delay. As apparent from the figure, the peaks shift differs for the time delays

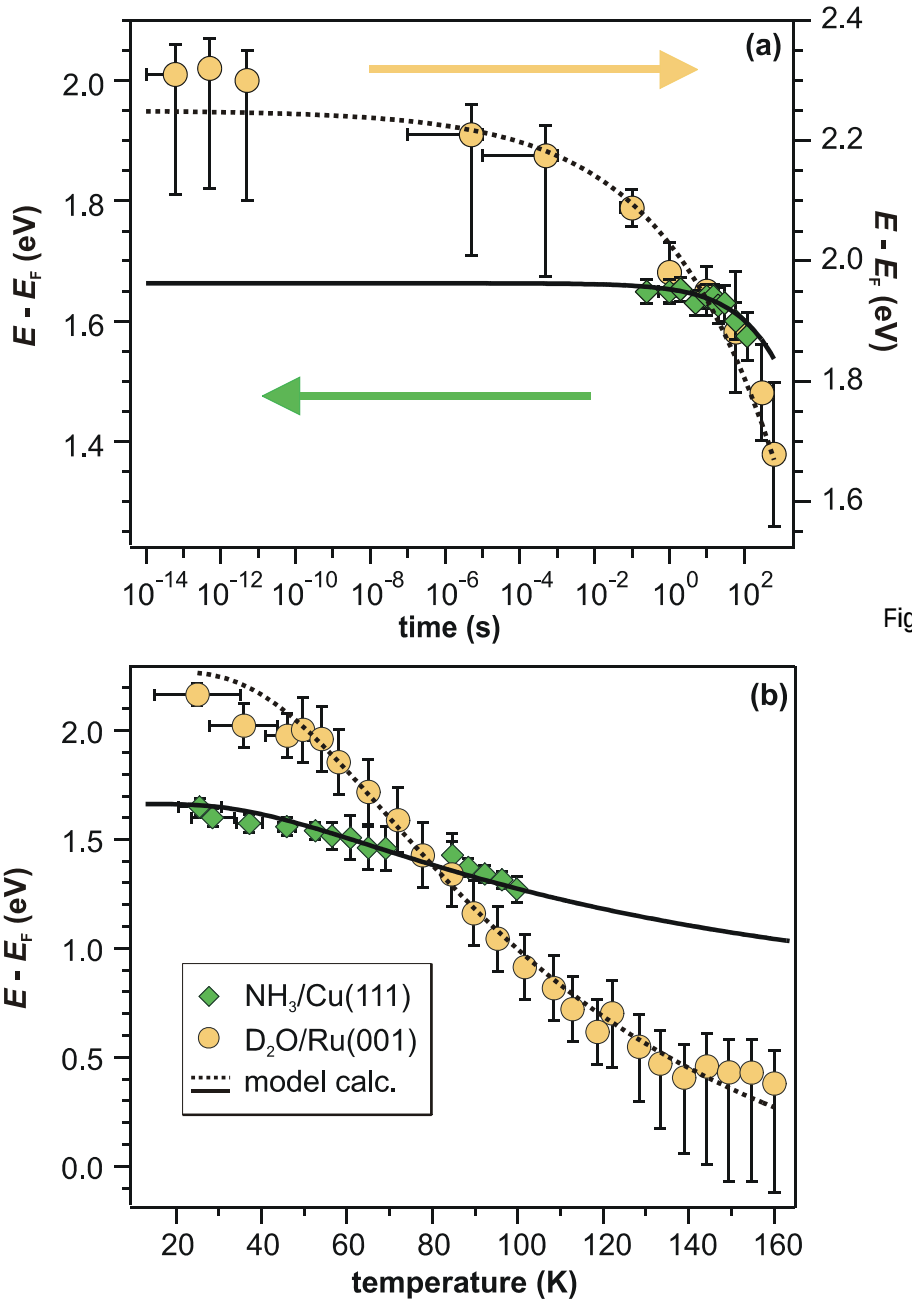

Fig. 5.24: *Comparison of the e_T Dynamics for NH_3 and D_2O.* a) Time-dependent shift of the peak maximum of the trapped electron distribution in ice (orange, right axis) and ammonia adlayers (green, left axis). b) Temperature-dependent peak shift. Dashed and solid lines result from the model calculation introduced in 4.2.2. See text for details.

investigated.[111] Fig. 5.24b presents the temperature-dependent peak shift of the ultralong-living electrons at the interfaces investigated. Apparently, the trapped electrons in NH_3/Cu(111) exhibit a considerably weaker temperature dependence. To quantitatively compare the data, the stretched exponential approach derived in paragraph 4.2.2 was used to analyze the time- and the energy-dependent peak shift at the NH_3/Cu(111) interface. As for ice (dashed curves), the function

$$E(t,T) = A \cdot q_0^2 \cdot \exp\left[-2 \cdot \exp\left(g(T) \cdot t^{\beta}\right)\right] + E_0 , \tag{5.8}$$

with

$$g(T) = \left(\tau_0^{-1} \cdot \exp\left[-\frac{E_a}{k_B T} \right] \right)^{\beta} \tag{5.9}$$

was fitted to both, time- and temperature-dependent peak shift (solid lines in Fig. 5.24). Obviously, the datasets can be excellently reproduced by the model calculation. The resulting fit parameters are depicted and compared with the ice values in Tab. 5.02. The exponent β, which stretches the real time t to the "internal clock" of the system $\tau = t^{\beta}$ (cf. 4.2.2), is larger for the NH_3Cu(111) interface. In other words, less stretching is required for the dynamics occurring in ammonia layers, i.e. the dynamics range over less timescales. The mean energy barrier for thermally activated stabilization of the excess electrons is with 32 meV smaller than for ice (96 meV). It was shown in paragraph 4.2.2, that solvation proceeds via conformational substates, which were identified to be flip rotations of the water molecules. The lowered barrier for NH_3 thus suggests that such CSS are separated by smaller barriers in crystalline ammonia. As the hydrogen bonding is weaker for solid ammonia than for crystalline ice (cf. 2.4.1), this result appears reasonable. The characteristic time τ_0 = 0.9 s is considerably higher for NH_3/Cu(111) than for the ice-metal interface (4 ms). As apparent from equation (5.9), it may be viewed as a weighting factor of time and temperature dependence of the stabilization dynamics: The larger it is, the smaller the impact of a temperature increase on the peak shift. As $g(T)$ can be viewed as a temperature-dependent friction coefficient of the whole solvation process, $(\tau_0)^{-1}$ is a measure for the friction that the solvated electron encounters for T = 0 K. Accordingly, the friction is smaller for ammonia, or – differently speaking – the hydrogen-bonded ammonia network is more flexible than the rigid crystalline D_2O structure.

	NH_3/Cu(111)	D_2O/Cu(111)
A/eV	1.65(10)	3.0(1)
E_a/meV	32(5)	96(5)
τ_0/s	0.9(1)	0.004(1)
β	0.4(1)	0.16(3)
E_0/eV	0.0(1)	-0.75(10)

Tab. 5.02: *Parameters of CSS Model.*

[111] For delays >120 s the low intensity of e_T in the case of NH_3/Cu(111) inhibits evaluation of the peak shift, as mentioned above. Investigation of the ultrafast dynamics of the trapped electron in ammonia adlayers is not performed in this work, as this sophisticated experiment, requiring enormous stability and resolution, could not be carried out in a reasonable period of time.

The amplitude A corresponds to the reorganization energy λ of the respective system, as

$$E(q) = A \cdot (q - q_0)^2 + E_0 . \tag{5.10}$$

Since A is smaller for the NH_3 adlayers, the energy cost of the lattice deformation for complete solvation of the excess charge, the reorganization energy λ, is larger for the ice network. Fig. 5.25 sketches the two different harmonic potentials of the two solvents ice (orange) and ammonia (green). The larger gradient for crystalline ice illustrates a stronger driving force for the electron solvation, which is the reason for the stronger peak shift (in time and energy) for the D_2O/Ru(001) interface.

However, these results are to be confirmed by time-resolved measurements of the *ultrafast* dynamics of the trapped electrons in ammonia on Cu(111). If the trapped electrons exhibit intermediate state energies of 1.65 eV as predicted by the model fit in Fig. 5.24a (solid curve), the above results are approved. In any case, it can be summarized, that the electron solvation dynamics in crystalline NH_3/Cu(111) exhibit qualitatively the same time- and temperature-dependent behavior. Quantitatively, however, the electron solvation is less pronounced for the ammonia adlayers.

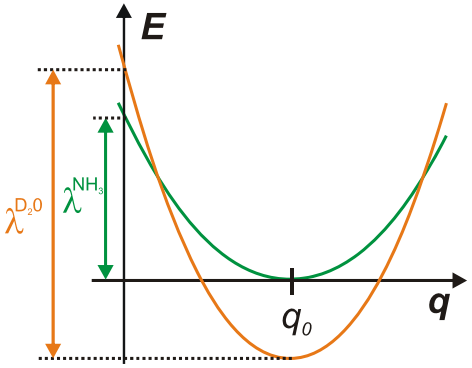

Fig. 5.25: *Harmonic Potentials of NH_3 and D_2O.*

Conclusions

Ultralong-living, trapped electrons were observed in crystalline ice and ammonia adlayers on metal surfaces. Due to their ultralong lifetimes on the order of minutes, it was possible to investigate the temporal evolution of the electron binding energy over 16 orders of magnitude in time, showing that stabilization is not completed even after minutes. The occurrence of dynamics from femtoseconds to minutes required implementation of a stretched exponential time-dependence – a well-known approach for protein folding in solvent environments. The trapped electrons exhibit for both investigated systems a temperature dependence; stronger in the case of ice, weaker for ammonia. It was shown in paragraph 4.2.2, that the stabilization dynamics in ice adlayers are well-described by stretched exponentials incorporating electron solvation via conformational substates (CSS), where progression along the solvation coordinate q occurs due to thermally activated molecular reorientation. Implementation of the stretched exponential behavior for the NH_3/Cu(111) resulted – amongst others – in a smaller activation barrier for thermally activated stabilization. Yet, despite the differences, it is remarkable, that such efficiently screened trapped electrons with extremely long lifetimes are apparently *not* and ice-specific characteristic. The observation of ultralong-living electrons in ammonia therefore

suggests that other solvents might be capable of trapping and localizing an excess charge at the adsorbate-vacuum interface.